EUROPEAN LABORATORY FOR PARTICLE PHYSICS

CERN-EP/98-167
19th October 1998

W^+W^- production and triple gauge boson couplings at LEP energies up to 183 GeV

The OPAL Collaboration

Abstract

A study of W-pair production in e^+e^- annihilations at LEP is presented, based on 877 W^+W^- candidates corresponding to an integrated luminosity of 57 pb^{-1} at $\sqrt{s}$=183 GeV. Assuming that the angular distributions of the W-pair production and decay, as well as their branching fractions, are described by the Standard Model, the W-pair production cross-section is measured to be 15.43±0.61(stat.)±0.26(syst.) pb. Assuming lepton universality and combining with our results from lower centre-of-mass energies, the W branching fraction to hadrons is determined to be 67.9±1.2(stat.)±0.5(syst.)%. The number of W-pair candidates and the angular distributions for each final state ($q\overline{q}\ell\nu_\ell$, $q\overline{q}q\overline{q}$, $\overline{\ell}\nu_\ell\ell'\overline{\nu}_{\ell'}$) are used to determine the triple gauge boson couplings. After combining these values with our results from lower centre-of-mass energies we obtain $\Delta\kappa_\gamma=0.11^{+0.52}_{-0.37}$, $\Delta g_1^z=0.01^{+0.13}_{-0.12}$ and $\lambda=-0.10^{+0.13}_{-0.12}$, where the errors include both statistical and systematic uncertainties and each coupling is determined setting the other two couplings to the Standard Model value. The fraction of W bosons produced with a longitudinal polarisation is measured to be 0.242±0.091(stat.)±0.023(syst.). All these measurements are consistent with the Standard Model expectations.

Submitted to the European Physical Journal C

The OPAL Collaboration

G. Abbiendi[2], K. Ackerstaff[8], G. Alexander[23], J. Allison[16], N. Altekamp[5], K.J. Anderson[9], S. Anderson[12], S. Arcelli[17], S. Asai[24], S.F. Ashby[1], D. Axen[29], G. Azuelos[18,a], A.H. Ball[17], E. Barberio[8], R.J. Barlow[16], R. Bartoldus[3], J.R. Batley[5], S. Baumann[3], J. Bechtluft[14], T. Behnke[27], K.W. Bell[20], G. Bella[23], A. Bellerive[9], S. Bentvelsen[8], S. Bethke[14], S. Betts[15], O. Biebel[14], A. Biguzzi[5], S.D. Bird[16], V. Blobel[27], I.J. Bloodworth[1], P. Bock[11], J. Böhme[14], D. Bonacorsi[2], M. Boutemeur[34], S. Braibant[8], P. Bright-Thomas[1], L. Brigliadori[2], R.M. Brown[20], H.J. Burckhart[8], P. Capiluppi[2], R.K. Carnegie[6], A.A. Carter[13], J.R. Carter[5], C.Y. Chang[17], D.G. Charlton[1,b], D. Chrisman[4], C. Ciocca[2], P.E.L. Clarke[15], E. Clay[15], I. Cohen[23], J.E. Conboy[15], O.C. Cooke[8], C. Couyoumtzelis[13], R.L. Coxe[9], M. Cuffiani[2], S. Dado[22], G.M. Dallavalle[2], R. Davis[30], S. De Jong[12], A. de Roeck[8], P. Dervan[15], K. Desch[8], B. Dienes[33,d], M.S. Dixit[7], J. Dubbert[34], E. Duchovni[26], G. Duckeck[34], I.P. Duerdoth[16], D. Eatough[16], P.G. Estabrooks[6], E. Etzion[23], F. Fabbri[2], M. Fanti[2], A.A. Faust[30], F. Fiedler[27], M. Fierro[2], I. Fleck[8], R. Folman[26], A. Fürtjes[8], D.I. Futyan[16], P. Gagnon[7], J.W. Gary[4], J. Gascon[18], S.M. Gascon-Shotkin[17], G. Gaycken[27], C. Geich-Gimbel[3], G. Giacomelli[2], P. Giacomelli[2], V. Gibson[5], W.R. Gibson[13], D.M. Gingrich[30,a], D. Glenzinski[9], J. Goldberg[22], W. Gorn[4], C. Grandi[2], K. Graham[28], E. Gross[26], J. Grunhaus[23], M. Gruwé[27], G.G. Hanson[12], M. Hansroul[8], M. Hapke[13], K. Harder[27], A. Harel[22], C.K. Hargrove[7], C. Hartmann[3], M. Hauschild[8], C.M. Hawkes[1], R. Hawkings[27], R.J. Hemingway[6], M. Herndon[17], G. Herten[10], R.D. Heuer[27], M.D. Hildreth[8], J.C. Hill[5], P.R. Hobson[25], M. Hoch[18], A. Hocker[9], K. Hoffman[8], R.J. Homer[1], A.K. Honma[28,a], D. Horváth[32,c], K.R. Hossain[30], R. Howard[29], P. Hüntemeyer[27], P. Igo-Kemenes[11], D.C. Imrie[25], K. Ishii[24], F.R. Jacob[20], A. Jawahery[17], H. Jeremie[18], M. Jimack[1], C.R. Jones[5], P. Jovanovic[1], T.R. Junk[6], D. Karlen[6], V. Kartvelishvili[16], K. Kawagoe[24], T. Kawamoto[24], P.I. Kayal[30], R.K. Keeler[28], R.G. Kellogg[17], B.W. Kennedy[20], D.H. Kim[19], A. Klier[26], S. Kluth[8], T. Kobayashi[24], M. Kobel[3,e], D.S. Koetke[6], T.P. Kokott[3], M. Kolrep[10], S. Komamiya[24], R.V. Kowalewski[28], T. Kress[4], P. Krieger[6], J. von Krogh[11], T. Kuhl[3], P. Kyberd[13], G.D. Lafferty[16], H. Landsman[22], D. Lanske[14], J. Lauber[15], S.R. Lautenschlager[31], I. Lawson[28], J.G. Layter[4], D. Lazic[22], A.M. Lee[31], D. Lellouch[26], J. Letts[12], L. Levinson[26], R. Liebisch[11], B. List[8], C. Littlewood[5], A.W. Lloyd[1], S.L. Lloyd[13], F.K. Loebinger[16], G.D. Long[28], M.J. Losty[7], J. Ludwig[10], D. Liu[12], A. Macchiolo[2], A. Macpherson[30], W. Mader[3], M. Mannelli[8], S. Marcellini[2], C. Markopoulos[13], A.J. Martin[13], J.P. Martin[18], G. Martinez[17], T. Mashimo[24], P. Mättig[26], W.J. McDonald[30], J. McKenna[29], E.A. Mckigney[15], T.J. McMahon[1], R.A. McPherson[28], F. Meijers[8], S. Menke[3], F.S. Merritt[9], H. Mes[7], J. Meyer[27], A. Michelini[2], S. Mihara[24], G. Mikenberg[26], D.J. Miller[15], R. Mir[26], W. Mohr[10], A. Montanari[2], T. Mori[24], K. Nagai[8], I. Nakamura[24], H.A. Neal[12], B. Nellen[3], R. Nisius[8], S.W. O'Neale[1], F.G. Oakham[7], F. Odorici[2], H.O. Ogren[12], M.J. Oreglia[9], S. Orito[24], J. Pálinkás[33,d], G. Pásztor[32], J.R. Pater[16], G.N. Patrick[20], J. Patt[10], R. Perez-Ochoa[8], S. Petzold[27], P. Pfeifenschneider[14], J.E. Pilcher[9], J. Pinfold[30], D.E. Plane[8], P. Poffenberger[28], J. Polok[8], M. Przybycień[8], C. Rembser[8], H. Rick[8], S. Robertson[28], S.A. Robins[22], N. Rodning[30], J.M. Roney[28], K. Roscoe[16], A.M. Rossi[2], Y. Rozen[22], K. Runge[10], O. Runolfsson[8], D.R. Rust[12], K. Sachs[10], T. Saeki[24], O. Sahr[34], W.M. Sang[25], E.K.G. Sarkisyan[23], C. Sbarra[29], A.D. Schaile[34], O. Schaile[34], F. Scharf[3], P. Scharff-Hansen[8], J. Schieck[11], B. Schmitt[8], S. Schmitt[11], A. Schöning[8], M. Schröder[8], M. Schumacher[3], C. Schwick[8], W.G. Scott[20], R. Seuster[14], T.G. Shears[8], B.C. Shen[4], C.H. Shepherd-Themistocleous[8], P. Sherwood[15], G.P. Siroli[2], A. Sittler[27], A. Skuja[17], A.M. Smith[8], G.A. Snow[17], R. Sobie[28], S. Söldner-Rembold[10], S. Spagnolo[20], M. Sproston[20], A. Stahl[3], K. Stephens[16], J. Steuerer[27], K. Stoll[10], D. Strom[19],

R. Ströhmer[34], B. Surrow[8], S.D. Talbot[1], S. Tanaka[24], P. Taras[18], S. Tarem[22], R. Teuscher[8], M. Thiergen[10], J. Thomas[15], M.A. Thomson[8], E. von Törne[3], E. Torrence[8], S. Towers[6], I. Trigger[18], Z. Trócsányi[33], E. Tsur[23], A.S. Turcot[9], M.F. Turner-Watson[1], I. Ueda[24], B. Vachon[28], R. Van Kooten[12], P. Vannerem[10], M. Verzocchi[10], H. Voss[3], F. Wäckerle[10], A. Wagner[27], C.P. Ward[5], D.R. Ward[5], P.M. Watkins[1], A.T. Watson[1], N.K. Watson[1], P.S. Wells[8], N. Wermes[3], J.S. White[6], G.W. Wilson[16], J.A. Wilson[1], T.R. Wyatt[16], S. Yamashita[24], G. Yekutieli[26], V. Zacek[18], D. Zer-Zion[8]

[1]School of Physics and Astronomy, University of Birmingham, Birmingham B15 2TT, UK
[2]Dipartimento di Fisica dell' Università di Bologna and INFN, I-40126 Bologna, Italy
[3]Physikalisches Institut, Universität Bonn, D-53115 Bonn, Germany
[4]Department of Physics, University of California, Riverside CA 92521, USA
[5]Cavendish Laboratory, Cambridge CB3 0HE, UK
[6]Ottawa-Carleton Institute for Physics, Department of Physics, Carleton University, Ottawa, Ontario K1S 5B6, Canada
[7]Centre for Research in Particle Physics, Carleton University, Ottawa, Ontario K1S 5B6, Canada
[8]CERN, European Organisation for Particle Physics, CH-1211 Geneva 23, Switzerland
[9]Enrico Fermi Institute and Department of Physics, University of Chicago, Chicago IL 60637, USA
[10]Fakultät für Physik, Albert Ludwigs Universität, D-79104 Freiburg, Germany
[11]Physikalisches Institut, Universität Heidelberg, D-69120 Heidelberg, Germany
[12]Indiana University, Department of Physics, Swain Hall West 117, Bloomington IN 47405, USA
[13]Queen Mary and Westfield College, University of London, London E1 4NS, UK
[14]Technische Hochschule Aachen, III Physikalisches Institut, Sommerfeldstrasse 26-28, D-52056 Aachen, Germany
[15]University College London, London WC1E 6BT, UK
[16]Department of Physics, Schuster Laboratory, The University, Manchester M13 9PL, UK
[17]Department of Physics, University of Maryland, College Park, MD 20742, USA
[18]Laboratoire de Physique Nucléaire, Université de Montréal, Montréal, Quebec H3C 3J7, Canada
[19]University of Oregon, Department of Physics, Eugene OR 97403, USA
[20]CLRC Rutherford Appleton Laboratory, Chilton, Didcot, Oxfordshire OX11 0QX, UK
[22]Department of Physics, Technion-Israel Institute of Technology, Haifa 32000, Israel
[23]Department of Physics and Astronomy, Tel Aviv University, Tel Aviv 69978, Israel
[24]International Centre for Elementary Particle Physics and Department of Physics, University of Tokyo, Tokyo 113-0033, and Kobe University, Kobe 657-8501, Japan
[25]Institute of Physical and Environmental Sciences, Brunel University, Uxbridge, Middlesex UB8 3PH, UK
[26]Particle Physics Department, Weizmann Institute of Science, Rehovot 76100, Israel
[27]Universität Hamburg/DESY, II Institut für Experimental Physik, Notkestrasse 85, D-22607 Hamburg, Germany
[28]University of Victoria, Department of Physics, P O Box 3055, Victoria BC V8W 3P6, Canada
[29]University of British Columbia, Department of Physics, Vancouver BC V6T 1Z1, Canada
[30]University of Alberta, Department of Physics, Edmonton AB T6G 2J1, Canada

[31]Duke University, Dept of Physics, Durham, NC 27708-0305, USA
[32]Research Institute for Particle and Nuclear Physics, H-1525 Budapest, P O Box 49, Hungary
[33]Institute of Nuclear Research, H-4001 Debrecen, P O Box 51, Hungary
[34]Ludwigs-Maximilians-Universität München, Sektion Physik, Am Coulombwall 1, D-85748 Garching, Germany

[a] and at TRIUMF, Vancouver, Canada V6T 2A3
[b] and Royal Society University Research Fellow
[c] and Institute of Nuclear Research, Debrecen, Hungary
[d] and Department of Experimental Physics, Lajos Kossuth University, Debrecen, Hungary
[e] on leave of absence from the University of Freiburg

1 Introduction

One of the main motivations to double the LEP energy was to study the W boson properties as well as the characteristics of the W-pair production process, such as the total cross-section, the angular distributions and the helicity structure. The total cross-section for different final states can be used to measure the W decay branching fractions in order to test lepton universality and to extract information about the Cabibbo-Kobayashi-Maskawa quark mixing matrix.

In addition to the t-channel ν-exchange, W-pair production in e^+e^- annihilations involves the triple gauge boson vertices WWγ and WWZ which are present in the Standard Model due to its non-Abelian nature. Therefore, all the W-pair production properties can be interpreted in terms of the Triple Gauge Couplings (TGCs). Any deviation from the Standard Model predictions would be evidence for new physics.

The most general Lorentz invariant Lagrangian [1–4] which describes the triple gauge boson interaction involving W bosons has fourteen independent terms, seven describing the WWγ vertex and seven describing the WWZ vertex. This parameter space is very large, and it is not currently possible to measure all fourteen couplings independently. Assuming that the Lagrangian satisfies electromagnetic gauge invariance and charge conjugation as well as parity invariance, the number of parameters reduces to five, which can be taken as g_1^z, κ_z, κ_γ, λ_z and λ_γ [1, 2]. In the Standard Model g_1^z=κ_z=κ_γ=1 and λ_z=λ_γ=0. Considerations related to SU(2)$\times$U(1) gauge invariance, supported by constraints arising from precise measurements on the Z^0 resonance and lower energy data, suggest the following relations between the five couplings [1, 3],

$$\begin{aligned} \Delta\kappa_z &= -\Delta\kappa_\gamma \tan^2\theta_w + \Delta g_1^z, \\ \lambda_z &= \lambda_\gamma, \end{aligned} \tag{1}$$

where the Δ indicates a deviation of the respective quantity from its Standard Model value and θ_w is the weak mixing angle. These constraints leave only three independent couplings[1], $\Delta\kappa_\gamma$, Δg_1^z and $\lambda(=\lambda_\gamma=\lambda_z)$ which are not significantly restricted [5, 6] by existing LEP Z^0 data.

First TGC studies were made at $\overline{\mathrm{p}}$p colliders, mainly at the Tevatron by CDF [7] and D0 [8], using di-boson production. Previous results from LEP used the data recorded at 161 GeV [9,10] and 172 GeV [11,12] with an integrated luminosity of $\approx$ 10 pb^{-1} at each centre-of-mass energy. Here we present an analysis of the OPAL data taken in 1997 at a centre-of-mass energy of 182.7 GeV. The TGC results are combined with those at lower centre-of-mass energies.

Anomalous TGCs affect both the total W-pair cross-section and the production angular distribution. Additionally, the relative contribution of each helicity state would be modified, which in turn affects the angular distributions of the W decay products.

In the limit of small W width and no initial state radiation (ISR), the production and decay of W bosons is characterised by five angles. These are conventionally [1, 3, 13] taken to be:

[1] In our previous publications we analysed the α parameters which are motivated by specific theoretical models and are given by, $\alpha_{B\phi}= \Delta\kappa_\gamma - \Delta g_1^z \cos^2\theta_w$, $\alpha_{W\phi}= \Delta g_1^z \cos^2\theta_w$ and $\alpha_W=\lambda$. In this paper, however, we prefer to use parameters which are directly related to the W electromagnetic and weak properties [2, 3].

the W^- production polar angle[2] θ_W; the polar and azimuthal angles, θ_1^* and ϕ_1^*, of the decay fermion, $W^-\to f$, in the W^- rest frame[3]; and the analogous angles for the $W^+\to\overline{f}$ decay, θ_2^* and ϕ_2^*. These five angles contain all the information which can be extracted about the helicity structure of W^+W^- production and decay. The effects of the finite W width and ISR are not large at a centre-of-mass energy of around 183 GeV [1]. However the experimental accessibility of the different angles in W^+W^- events observed in the detector, and therefore the sensitivity to the TGCs, depends strongly on the final states produced when the W boson decays.

In this paper we analyse W-pairs in all possible final states, namely, $W^+W^-\to q\overline{q}\overline{\ell}\nu_\ell$, where one W boson decays into hadrons and the other decays into leptons[4], $W^+W^-\to q\overline{q}q\overline{q}$, where both W bosons decay hadronically, and $W^+W^-\to \overline{\ell}\nu_\ell\ell'\overline{\nu}_{\ell'}$, where both W bosons decay into leptons.

Most of the TGC results of this analysis are obtained for each of the three couplings separately, setting the other two couplings to zero which is the Standard Model value. These results will be presented in tables and $\log L$ curves[5]. We also perform two-dimensional and three dimensional fits, where two or all three TGC parameters are allowed to vary in the fits. The results of these fits will be presented by contour plots.

The following section includes a short presentation of the OPAL data and Monte Carlo samples, and in section 3 the selection of our W-pair sample is described. The analysis of the W-pair cross-section and the W decay branching fractions is presented in section 4, along with the interpretation of this analysis in terms of the TGCs. The TGC analysis using the angular distributions is done separately for each channel and is described in sections 5, 6 and 7. The combined TGC results are presented in section 8. Section 9 includes the summary and conclusions of this study.

2 Data and Monte Carlo models

A detailed description of the OPAL detector has been presented elsewhere [14,15]. The accepted integrated luminosity in 1997, evaluated using small angle Bhabha scattering events observed in the silicon tungsten forward calorimeter, is 57.21 $\pm$0.15 $\pm$0.20 pb^{-1} where the first error is statistical and the second systematic. The luminosity-weighted mean centre-of-mass energy for the data sample is $\sqrt{s}$=182.68$\pm$0.05 GeV. Part of the TGC analysis involves the 161 and 172 GeV data samples taken in 1996 at centre-of-mass energies of 161.33$\pm$0.05 and 172.12$\pm$0.06 GeV with corresponding luminosities of 9.89$\pm$0.06 and 10.36$\pm$0.06 pb^{-1}.

The semi-analytic program GENTLE [16] is used to calculate the W^+W^- cross-section for the

[2] The OPAL right-handed coordinate system is defined such that the origin is at the geometric centre of the detector, the z-axis is parallel to, and has positive sense, along the e^- beam direction, θ is the polar angle with respect to z and ϕ is the azimuthal angle around z.

[3] The axes of the right-handed coordinate system in the W rest-frame are defined such that z is along the parent W flight direction and y is in the direction $\overrightarrow{e^-}\times\overrightarrow{W}$ where $\overrightarrow{e^-}$ is the electron beam direction and $\overrightarrow{W}$ is the parent W flight direction.

[4] Throughout this paper charge conjugate modes are also included and $q\overline{q}$ implicitly means any pair of quark-antiquark of different (or same) flavour which can be produced in W (Z^0) decay.

[5] Throughout this paper, $\log L$ denotes negative log-likelihood.

Standard Model case and also for different values of anomalous TGCs. The calculated Standard Model cross-section is 15.72 pb at $\sqrt{s}$=182.68 GeV using the W mass of $M_{\rm W}$=80.40 GeV/c^2 measured at the Tevatron[6] [17].

In the analyses described below, a number of Monte Carlo models are used to provide estimates of efficiencies and backgrounds as well as the expected W-pair production and decay angular distributions for different TGC values. The majority of the Monte Carlo samples were generated at $\sqrt{s}$ = 183 GeV with $M_{\rm W}$ = 80.33 GeV/c^2. All Monte Carlo samples mentioned below, unless referred to as "generator level", were passed through the full OPAL simulation program [18] and then subjected to the same reconstruction procedure as the data.

A Monte Carlo sample of signal events for the cross-section analysis was produced by the KORALW [19] generator with $\rm W^+W^-$ production diagrams (class[7] CC03) according to the Standard Model. The KORALW generator has the most accurate simulation of ISR and a complete treatment of tau polarisation in $\rm q\overline{q}\tau\overline{\nu}_\tau$ events. This sample is used to estimate the W-pair selection efficiency. Other Monte Carlo samples used for systematic checks were generated with the same set of diagrams using the EXCALIBUR [20] and `grc4f` [21] programs. To estimate the hadronization systematics, Monte Carlo samples were produced by the PYTHIA [22] and HERWIG [23] generators.

The TGC studies rely mainly on the EXCALIBUR program which has been used to generate samples with anomalous TGCs in order to calculate the TGC dependence of the selection efficiency and to obtain the expected angular distributions used in the TGC analysis.

The separation between signal and background processes is complicated by the interference between the CC03 set of W-pair production diagrams and other four-fermion graphs, such as $\rm e^+e^- \to We\overline{\nu}_e$, $\rm e^+e^- \to Z^0e^+e^-$ and $\rm e^+e^- \to Z^0Z^0$. To study the influence of interference effects in the four-fermion final states, the `grc4f` and EXCALIBUR Monte Carlo generators are used. In both cases samples were generated using the full set of interfering four-fermion diagrams. These four-fermion samples were compared to samples obtained with the same generator using only the CC03 diagrams. Four-fermion samples were generated also with anomalous TGCs.

Other background sources do not interfere with the signal. The main one, $\rm Z^0/\gamma \to q\overline{q}$, including higher order QCD diagrams, is simulated using PYTHIA, with HERWIG used as an alternative to study possible systematic effects. Other background processes involving two fermions in the final state are studied using KORALZ [24] for $\rm e^+e^- \to \mu^+\mu^-$, $\rm e^+e^- \to \tau^+\tau^-$ and $\rm e^+e^- \to \nu\overline{\nu}$, and BHWIDE [25] for $\rm e^+e^- \to e^+e^-$. Backgrounds from two-photon processes are evaluated using PYTHIA, HERWIG, PHOJET [26] and the Vermaseren generator [27]. It is assumed that the present centre-of-mass energy of 183 GeV is below the threshold for Higgs boson production.

[6] The LEP results for the W mass are not used for the TGC measurement, since they have been obtained under the assumption that W pairs are produced according to the Standard Model, whereas W production at the Tevatron does not involve the triple gauge vertex.

[7] In this paper, the W pair production diagrams, *i.e.* t-channel $\nu_{\rm e}$ exchange and s-channel $\rm Z^0/\gamma$ exchange, are referred to as "CC03", following the notation of [1].

3 Event selection

W-pair events decay into fully leptonic ($\mathrm{W^+W^-} \to \overline{\ell}\nu_\ell \ell'\overline{\nu}_{\ell'}$), semi-leptonic ($\mathrm{W^+W^-} \to \mathrm{q\overline{q}}\overline{\ell}\nu_\ell$) and fully hadronic ($\mathrm{W^+W^-} \to \mathrm{q\overline{q}q\overline{q}}$) final states with expected branching fractions of 10.5%, 43.9% and 45.6%, respectively. The $\mathrm{W^+W^-}$ event selection consists of three distinct parts to identify each of these topologies. The selections used at 183 GeV are based upon those used in the OPAL analysis at $\sqrt{s} \approx 172$ GeV [28]. The three selections are exclusive. Only events failing the $\mathrm{W^+W^-} \to \overline{\ell}\nu_\ell \ell'\overline{\nu}_{\ell'}$ selection are considered as possible $\mathrm{W^+W^-} \to \mathrm{q\overline{q}}\overline{\ell}\nu_\ell$ candidates and only events failing both the $\mathrm{W^+W^-} \to \overline{\ell}\nu_\ell \ell'\overline{\nu}_{\ell'}$ and $\mathrm{W^+W^-} \to \mathrm{q\overline{q}}\overline{\ell}\nu_\ell$ selections are considered as possible $\mathrm{W^+W^-} \to \mathrm{q\overline{q}q\overline{q}}$ candidates. The fully leptonic and semi-leptonic selections are separated into the individual lepton types to test charged current lepton universality.

The detailed selection algorithms are described below. The efficiency values and accepted background cross sections are summarised in Tables 1 and 2.

Event selection	Efficiencies[%] for $\mathrm{W^+W^-} \to$ $\mathrm{e^+\nu_e e^-\overline{\nu}_e}$	$\mathrm{e^+\nu_e}\mu^-\overline{\nu}_\mu$	$\mathrm{e^+\nu_e}\tau^-\overline{\nu}_\tau$	$\mu^+\nu_\mu\mu^-\overline{\nu}_\mu$	$\mu^+\nu_\mu\tau^-\overline{\nu}_\tau$	$\tau^+\nu_\tau\tau^-\overline{\nu}_\tau$	$\mathrm{q\overline{q}e\overline{\nu}_e}$	$\mathrm{q\overline{q}}\mu\overline{\nu}_\mu$	$\mathrm{q\overline{q}}\tau\overline{\nu}_\tau$	$\mathrm{q\overline{q}q\overline{q}}$
$\mathrm{e^+\nu_e e^-\overline{\nu}_e}$	67.3	0.2	6.5	0.0	0.0	0.6	0.0	0.0	0.0	0.0
$\mathrm{e^+\nu_e}\mu^-\overline{\nu}_\mu$	2.2	69.9	5.5	0.5	5.8	1.2	0.0	0.0	0.0	0.0
$\mathrm{e^+\nu_e}\tau^-\overline{\nu}_\tau$	12.2	8.7	58.2	0.0	1.6	8.9	0.0	0.0	0.0	0.0
$\mu^+\nu_\mu\mu^-\overline{\nu}_\mu$	0.0	1.2	0.1	73.7	5.7	0.6	0.0	0.0	0.0	0.0
$\mu^+\nu_\mu\tau^-\overline{\nu}_\tau$	0.1	3.5	0.6	10.8	56.4	6.8	0.0	0.0	0.0	0.0
$\tau^+\nu_\tau\tau^-\overline{\nu}_\tau$	0.7	0.9	4.9	1.3	6.2	44.1	0.0	0.0	0.0	0.0
$\mathrm{q\overline{q}e\overline{\nu}_e}$	0.0	0.0	0.1	0.0	0.0	0.1	84.0	0.1	5.8	0.1
$\mathrm{q\overline{q}}\mu\overline{\nu}_\mu$	0.0	0.0	0.0	0.0	0.1	0.0	0.1	86.2	4.5	0.2
$\mathrm{q\overline{q}}\tau\overline{\nu}_\tau$	0.0	0.0	0.0	0.0	0.0	0.1	4.5	4.5	64.6	0.6
$\mathrm{q\overline{q}q\overline{q}}$	0.0	0.0	0.0	0.0	0.0	0.0	0.0	0.0	0.5	84.6

Table 1: Efficiency matrix for the 183 GeV event selections determined using KORALW (CC03) Monte Carlo events. Each entry represents the percentage of generated events for each decay channel which are accepted by the different selections.

The first six background sources listed in Table 2 are different four-fermion final states. Their expected cross-sections include both contributions from non-CC03 diagrams and the effects of interference. The four-fermion background cross-sections for each final state are calculated from the difference between the accepted four-fermion cross-section including all diagrams, and the accepted CC03 cross-section. For this determination the `grc4f` Monte Carlo generator is used. The associated systematic uncertainty is estimated by comparing the predictions of `grc4f` and EXCALIBUR. At the current level of statistical precision such interference effects are small within our experimental angular acceptance.

	Accepted background cross-sections (fb) Event Selection $W^+W^- \rightarrow$				
Source	$\overline{\ell}\nu_\ell\ell'\overline{\nu}_{\ell'}$	$q\overline{q}e\overline{\nu}_e$	$q\overline{q}\mu\overline{\nu}_\mu$	$q\overline{q}\tau\overline{\nu}_\tau$	$q\overline{q}q\overline{q}$
$q\overline{q}q\overline{q}$	0 ± 0	2 ± 2	1 ± 2	6 ± 4	220 ± 50
$q\overline{q}e\overline{\nu}_e$	0 ± 0	56 ± 28	1 ± 1	53 ± 11	0 ± 0
$q\overline{q}\ell\overline{\ell}$	0 ± 0	65 ± 19	29 ± 4	74 ± 7	72 ± 6
$q\overline{q}\nu\overline{\nu}$	0 ± 0	0 ± 0	0 ± 0	12 ± 3	0 ± 0
$\ell\overline{\ell}\nu\overline{\nu}$	40 ± 23	0 ± 0	0 ± 0	0 ± 0	0 ± 0
$\ell\overline{\ell}\ell\overline{\ell}$	9 ± 2	1 ± 1	0 ± 0	1 ± 1	0 ± 0
$Z^0/\gamma \rightarrow q\overline{q}$	0 ± 0	61 ± 17	28 ± 6	183 ± 22	1370 ± 150
$Z^0/\gamma \rightarrow \ell\overline{\ell}$	6 ± 1	2 ± 1	1 ± 1	6 ± 2	0 ± 0
Two-photon	30 ± 30	13 ± 13	0 ± 0	5 ± 5	6 ± 6
Combined	85 ± 38	200 ± 40	60 ± 8	340 ± 27	1670 ± 160

Table 2: Background cross-sections for the 183 GeV W^+W^- selections. The values for the $q\overline{q}q\overline{q}$, $q\overline{q}e\overline{\nu}_e$ and $\overline{\ell}\nu_\ell\ell'\overline{\nu}_{\ell'}$ sources are obtained from the difference between the full four-fermion and the corresponding CC03 cross-sections. All errors include both statistical and systematic contributions.

3.1 $W^+W^- \rightarrow \overline{\ell}\nu_\ell\ell'\overline{\nu}_{\ell'}$ event selection

Fully leptonic W^+W^- events are identified as an acoplanar pair of charged leptons with missing momentum. The event selection is unchanged from that used in reference [28] (described in detail in [29]). In the $\sqrt{s} \approx 183$ GeV data sample, 78 events are selected as $W^+W^- \rightarrow \overline{\ell}\nu_\ell\ell'\overline{\nu}_{\ell'}$ candidates.

The selection efficiency is estimated to be $(78.0 \pm 2.3)\%$ where the error includes systematic uncertainties. The efficiencies for the individual channels are given in Table 1. The dominant systematic uncertainty on the selection efficiency arises from differences observed when comparing Monte Carlo samples which have different implementations of both initial and final state radiation effects and the modelling of tau decays. In addition, systematic errors were included to account for data/Monte Carlo disagreement (0.8%), the possibility of events being rejected due to off-momentum beam particles which can deposit significant energy in the forward detectors (0.5%), and the knowledge of the trigger efficiency (0.4%). The expected background cross-sections from Standard Model processes are given in Table 2.

3.2 $W^+W^- \rightarrow q\overline{q}\overline{\ell}\nu_\ell$ event selection

The $W^+W^- \rightarrow q\overline{q}\overline{\ell}\nu_\ell$ selection consists of three separate selections, one for each lepton flavour. The $W^+W^- \rightarrow q\overline{q}\tau\overline{\nu}_\tau$ selection is applied only to events which fail both the $W^+W^- \rightarrow q\overline{q}e\overline{\nu}_e$ and $W^+W^- \rightarrow q\overline{q}\mu\overline{\nu}_\mu$ selections.

The $W^+W^- \rightarrow q\overline{q}\overline{\ell}\nu_\ell$ event selection for the 183 GeV data is a modified version of the 172 GeV selection described in detail in [28]. A looser set of preselection cuts is used since the lepton energy spectrum is broader at 183 GeV due to the increased boost. The set of variables used in the likelihood selections has been also modified. In the $W^+W^- \rightarrow q\overline{q}\tau\overline{\nu}_\tau$ sample there is a significant background from hadronic decays of single-W four-fermion events ($e^+e^- \to We\overline{\nu}_e$) and an additional likelihood selection is used to reduce this. This selection is only applied to $W^+W^- \to q\overline{q}\tau\overline{\nu}_\tau$ events where the tau is identified as decaying in the single-prong hadronic channel. Finally, in order to reduce the $e^+e^- \to Z^0Z^0$ background, events passing the $W^+W^- \to q\overline{q}e\overline{\nu}_e$ likelihood selection are rejected if there is evidence for a second energetic electron. A similar procedure is applied to the $W^+W^- \to q\overline{q}\mu\overline{\nu}_\mu$ selection.

In total, 361 events are identified as $W^+W^- \to q\overline{q}\ell\nu_\ell$ candidates, of which 140 are selected as $W^+W^- \to q\overline{q}e\overline{\nu}_e$, 120 as $W^+W^- \to q\overline{q}\mu\overline{\nu}_\mu$ and 101 as $W^+W^- \to q\overline{q}\tau\overline{\nu}_\tau$. The efficiencies of the $W^+W^- \to q\overline{q}\ell\nu_\ell$ selection for the individual channels are given in Table 1. The efficiencies include corrections ($\approx 0.5\%$) which account for observed differences between the data and the Monte Carlo simulation as described in [28]. The efficiencies are also corrected by a factor of 0.991 ± 0.003 for the $W^+W^- \to q\overline{q}e\overline{\nu}_e$ and $W^+W^- \to q\overline{q}\mu\overline{\nu}_\mu$ selections and by a factor of 0.985 ± 0.005 for the $W^+W^- \to q\overline{q}\tau\overline{\nu}_\tau$ selection to account for events being rejected due to the presence of off-momentum beam particles which can deposit significant energy in the forward detectors. A systematic error is assigned for possible tracking losses which are not modelled by the Monte Carlo simulation of the OPAL detector. This uncertainty is evaluated using selections designed to identify $W^+W^- \to q\overline{q}e\overline{\nu}_e$ and $W^+W^- \to q\overline{q}\mu\overline{\nu}_\mu$ events where the track was either not reconstructed or was poorly measured. Possible biases due to fragmentation uncertainties are studied by comparing fully simulated Monte Carlo $W^+W^- \to q\overline{q}\ell\nu_\ell$ samples with fragmentation performed using Pythia and Herwig. Other systematics are estimated using samples generated with different Monte Carlo models and different input W boson masses and beam energies. Table 3 lists the sources of the systematic uncertainties on the selection efficiencies.

		Signal efficiency error (%) Event selection $W^+W^- \to$			
	Source of uncertainty	$q\overline{q}e\overline{\nu}_e$	$q\overline{q}\mu\overline{\nu}_\mu$	$q\overline{q}\tau\overline{\nu}_\tau$	$q\overline{q}q\overline{q}$
a)	Statistical	0.3	0.3	0.4	0.2
b)	Comparison of MC models	0.6	0.4	0.5	0.3
c)	Data/Monte Carlo	0.6	0.5	0.6	0.6
d)	Tracking losses	0.4	0.4	0.4	–
e)	Detector occupancy	0.3	0.3	0.3	–
f)	Fragmentation	0.2	0.1	0.6	0.8
g)	M_W dependence (± 0.09 GeV/c^2)	0.1	0.2	0.1	0.1
h)	Beam energy dependence	0.1	0.1	0.1	0.1
	Combined	1.1	0.9	1.2	1.0

Table 3: Sources of uncertainty on the $W^+W^- \to q\overline{q}\ell\nu_\ell$ and $W^+W^- \to q\overline{q}q\overline{q}$ selection efficiencies.

Table 2 shows the corrected background cross-sections and their total uncertainties for the three $q\overline{q}\ell\nu_\ell$ selections. The systematic errors on the expected background cross-sections are dominated by differences between data and Monte Carlo for the two-fermion backgrounds and by differences between generators in the case of the four-fermion backgrounds. The systematic errors on the four-fermion backgrounds were estimated by comparing the expectations of `grc4f`, Excalibur and Pythia.

An initial estimate of the $Z^0/\gamma \to q\overline{q}$ background is obtained from Monte Carlo. This estimate is then corrected using data to account for possible uncertainties in the Monte Carlo modelling, *e.g.* the lepton fake rate in $Z^0/\gamma \to q\overline{q}$ events. Several methods are used to estimate the correction factors to the Monte Carlo estimates of the $Z^0/\gamma \to q\overline{q}$ background. The central value is obtained using 'fake' $Z^0/\gamma \to q\overline{q}$ events formed by boosting $Z^0 \to q\overline{q}$ events from at $\sqrt{s} = 91.2$ GeV along the z-axis according to the invariant mass distribution of the hadronic system in $Z^0/\gamma \to q\overline{q}$ events at $\sqrt{s}$=183 GeV [30]. This procedure is applied to both data and Monte Carlo. The correction factor is determined from the relative fractions (data/Monte Carlo) of 'fake' events which pass the $W^+W^- \to q\overline{q}\ell\nu_\ell$ selections. As a result, the Monte Carlo estimates of the $Z^0/\gamma \to q\overline{q}$ background are scaled by a factor of 1.3 ± 0.3 for the $W^+W^- \to q\overline{q}e\overline{\nu}_e$ selection, 1.0 ± 0.1 for the $W^+W^- \to q\overline{q}\mu\overline{\nu}_\mu$ selection and by 1.1 ± 0.1 for the $W^+W^- \to q\overline{q}\tau\overline{\nu}_\tau$ selection. The errors reflect the spread of values obtained using alternative methods, *e.g.* using events passing the preselection and then fitting Monte Carlo signal ($W^+W^- \to q\overline{q}\overline{\ell}\nu_\ell$) and background ($Z^0/\gamma \to q\overline{q}$) components to the kinematic distributions of the data.

In the $W^+W^- \to q\overline{q}\tau\overline{\nu}_\tau$ selection there is a non-negligible background from hadronic decays of single-W events ($e^+e^- \to We\overline{\nu}_e$) where the electron goes undetected down the beam pipe. This background is determined by the number of fake tau candidates formed out of the fragmentation products in the hadronic decay of the W. A correction factor to the Monte Carlo background is obtained using fake single-W events formed by removing the lepton candidate from selected $W^+W^- \to q\overline{q}e\overline{\nu}_e$ and $W^+W^- \to q\overline{q}\mu\overline{\nu}_\mu$ events (both in data and Monte Carlo). The ratio of $W^+W^- \to q\overline{q}\tau\overline{\nu}_\tau$ selection efficiencies (data/Monte Carlo) for these fake events, 0.8 ± 0.1, is used to scale the Monte Carlo estimate of the $e^+e^- \to We\overline{\nu}_e$ background.

3.3 $W^+W^- \to q\overline{q}q\overline{q}$ event selection

The selection of fully hadronic $W^+W^- \to q\overline{q}q\overline{q}$ events is performed in two stages using a cut-based preselection followed by a likelihood selection procedure. The general features of this selection are similar to those used previously at 172 GeV [28], although it has been re-optimised to improve the rejection of the dominant background arising from hadronic $Z^0 \to q\overline{q}$ decays.

All events which are classified as hadronic events [31] and which have not been selected by either the $W^+W^- \to \overline{\ell}\nu_\ell\ell'\overline{\nu}_{\ell'}$ or $W^+W^- \to q\overline{q}\overline{\ell}\nu_\ell$ selections are considered as candidates for the $W^+W^- \to q\overline{q}q\overline{q}$ selection. Tracks and calorimeter clusters are combined into four jets using the Durham $k_\perp$ algorithm [32] and the total momentum and energy of each of the jets are corrected for double-counting of energy [33]. To remove events which are clearly inconsistent with a hadronic $W^+W^- \to q\overline{q}q\overline{q}$ decay, candidate events are required to satisfy the following preselection criteria:

- The fitted invariant mass of the event scaled by the collision energy, $\sqrt{s'/s}$, must be greater than 0.75.
- The visible energy of the event must be greater than $0.7\sqrt{s}$.
- The energy of the most energetic electromagnetic cluster must be less than $0.3\sqrt{s}$.
- Each jet is required to contain at least one charged track.

- The quantity[8] j_{ang} must be greater than 0.05.
- The logarithm of the QCD matrix element W_{420} [34], calculated using the jet momenta as estimates of the parton momenta, is required to be less than zero. W_{420} is an event weight formed from the tree level $O(\alpha_s^2)$ matrix element [35] for the QCD process ($\mathrm{e^+e^-} \rightarrow \mathrm{q\overline{q}q\overline{q}}, \mathrm{q\overline{q}gg}$). It is assigned the largest value of any permutation of associated jets to partons.

This preselection rejects 97.7% of the $\mathrm{Z^0} \rightarrow \mathrm{q\overline{q}}$ events which comprise the dominant background in the $\mathrm{W^+W^-} \rightarrow \mathrm{q\overline{q}q\overline{q}}$ channel. The preselection efficiency for the hadronic $\mathrm{W^+W^-} \rightarrow \mathrm{q\overline{q}q\overline{q}}$ decays is estimated to be 88.8%. In total, 524 candidates pass the preselection.

Events satisfying the preselection cuts are classified as signal or background based upon a four variable likelihood selection. The following likelihood variables are used since they provide a good separation between the hadronic $\mathrm{W^+W^-} \rightarrow \mathrm{q\overline{q}q\overline{q}}$ signal and the dominant $\mathrm{Z^0} \rightarrow \mathrm{q\overline{q}}$ background process for a minimum number of variables used:

- $\log(y_{45})$, the logarithm of the value of the Durham jet resolution parameter at which an event is reclassified from four jets to five jets.
- $\log(W_{420})$, the logarithm of the QCD matrix element [34].
- $|\cos\theta_{\mathrm{N-R}}|$, the cosine of the modified Nachtmann-Reiter angle[9] [36].
- the sphericity of the event.

Rather than using the product of the individual probability density functions to construct a classic likelihood discriminator, a coordinate transformation technique has been developed to reduce correlations between the four input variables [37].

An event is then selected as a hadronic $\mathrm{W^+W^-} \rightarrow \mathrm{q\overline{q}q\overline{q}}$ decay if the likelihood discriminant variable L, shown for data and Monte Carlo in Figure 1, is greater than 0.36. This cut value was chosen to maximise the product of signal purity and efficiency.

In the OPAL 172 GeV cross-section measurement [28], a 5% improvement in the statistical error was achieved by counting the event weights of all preselected events rather than simply specifying a cut on the discriminant variable. In this analysis, the use of event weights improves the statistical error on the cross-section measurement by less than 2% and results in an increased systematic uncertainty. For this reason, the more straightforward counting method is used.

The overall efficiency of the $\mathrm{W^+W^-} \rightarrow \mathrm{q\overline{q}q\overline{q}}$ event selection is estimated from the KORALW Monte Carlo simulation to be (84.6±1.0)% where the error is an estimate of all known systematic

[8] With the jets ordered by energy, the quantity j_{ang} is defined as $\frac{E_4}{\sqrt{s}}(1 - c_{12}c_{13}c_{23})$ where $c_{ij} = \cos\theta_{ij}$, θ_{ij} being the angle between jets i and j, and E_4 is the energy of the fourth (lowest energy) jet. This quantity is strongly peaked towards zero for the dominant $\mathrm{Z^0}/\gamma \rightarrow \mathrm{q\overline{q}}$ background process.

[9] With the jets ordered by energy, the quantity $\cos\theta_{\mathrm{N-R}}$ is defined as $\frac{(\vec{p}_1-\vec{p}_2)\cdot(\vec{p}_3-\vec{p}_4)}{|\vec{p}_1-\vec{p}_2||\vec{p}_3-\vec{p}_4|}$. This variable, which is sensitive to correlations between the underlying parton momenta, tends to be flat for the dominant $\mathrm{Z^0}/\gamma \rightarrow \mathrm{q\overline{q}}$ background and somewhat peaked for the $\mathrm{W^+W^-} \rightarrow \mathrm{q\overline{q}q\overline{q}}$ signal events.

uncertainties; the individual components are listed in Table 3. The total expected background cross-section from non-CC03 diagrams is estimated to be (1.67 ± 0.16) pb where the error represents the systematic uncertainty. The processes contributing to the background cross-section are listed in Table 2. In total, 438 candidates pass the selection.

The main source of uncertainty for both the signal efficiency and the background cross-section is related to the modelling of the fragmentation process. This uncertainty is estimated by comparing the selection efficiency for both signal and background events using an alternative QCD Monte Carlo model (HERWIG). In addition, the parameters σ_q, b, Λ_{QCD}, and Q_0 of the JETSET fragmentation model are varied by one standard deviation about their tuned values [38]. The Monte Carlo modelling of the data is further studied by comparing the distributions of the four likelihood variables seen in the data with various Monte Carlo samples. The signal efficiency evaluated using KORALW is compared to alternate generators (EXCALIBUR, PYTHIA and `grc4f`) to test the Monte Carlo description of the underlying hard process. Uncertainties related to the beam energy and W mass are evaluated with PYTHIA samples generated over a range of values. In each case, the observed differences are taken as an estimate of the systematic uncertainty.

4 W^+W^- cross-section and W decay branching fractions

4.1 Cross-section and branching fraction results

The observed numbers of selected W^+W^- events are used to measure the W^+W^- production cross-section and the W decay branching fractions to leptons and hadrons. The measured cross-section corresponds to that for W pair production via the CC03 diagrams.

Selected as	Efficiency [%]	Purity [%]	Expected	Observed
$W^+W^- \to \bar{\ell}\nu_\ell \ell' \bar{\nu}_{\ell'}$	78.0 ± 2.3	93.8	78.9 ± 2.3	78
$W^+W^- \to q\bar{q}\bar{\ell}\nu_\ell$	84.7 ± 1.3	90.2	371.2 ± 8.2	361
$W^+W^- \to q\bar{q}q\bar{q}$	84.6 ± 1.0	78.3	442.6 ± 12.4	438
Combined	84.4 ± 0.8	85.2	892.7 ± 19.2	877

Table 4: Observed numbers of candidate events in each W^+W^- decay topology for an integrated luminosity of (57.21 ± 0.25) pb^{-1} at (182.68 ± 0.05) GeV, together with expected numbers of events, assuming $M_W = (80.40 \pm 0.09)$ GeV/c^2 and Standard Model branching fractions. The expected numbers of events include systematic uncertainties from the efficiency, luminosity, beam energy, W^+W^- cross-section (2%) and M_W. In this table cross contamination between W^+W^- events from different topologies has been included as background (*i.e.* excluded from the efficiency numbers). The errors on the combined numbers account for correlations.

Table 4 summarises the event selections in the three W^+W^- decay topologies. The efficiencies refer to CC03 W^+W^- events. The expected number of events is calculated using the GENTLE cross-section of 15.72 pb assuming a W mass of 80.40 GeV/c^2 [17] and a centre-of-mass energy of 182.68 GeV. The systematic uncertainties on the expected numbers of events include contributions from the current errors of ± 0.09 GeV/c^2 on M_W and ± 0.05 GeV on the centre-of-mass energy (both below 0.1%) and a 2% theoretical uncertainty on the cross-section calculation. The data are consistent with the Monte Carlo expectation.

The selected numbers of events can be used to determine the W^+W^- CC03 production cross-sections separately into each channel:

$$\begin{aligned}
\sigma(W^+W^- \to \bar{\ell}\nu_\ell \ell'\bar{\nu}_{\ell'}) &= (1.64 \pm 0.20 \pm 0.07)\ \text{pb}, \\
\sigma(W^+W^- \to q\bar{q}\bar{\ell}\nu_\ell) &= (6.68 \pm 0.39 \pm 0.12)\ \text{pb}, \\
\sigma(W^+W^- \to q\bar{q}q\bar{q}) &= (7.07 \pm 0.43 \pm 0.21)\ \text{pb}.
\end{aligned}$$

As in [28], the W^+W^- cross-section and branching fractions are measured using the observed events from the ten separate channels summarised in Table 5. Three different maximum likelihood fits are performed. In the first case, $\sigma_{WW}(183\ \text{GeV})$, $\text{Br}(W \to e\bar{\nu}_e)$, $\text{Br}(W \to \mu\bar{\nu}_\mu)$ and $\text{Br}(W \to \tau\bar{\nu}_\tau)$ are extracted under the assumption that

$$\text{Br}(W \to e\bar{\nu}_e) + \text{Br}(W \to \mu\bar{\nu}_\mu) + \text{Br}(W \to \tau\bar{\nu}_\tau) + \text{Br}(W \to q\bar{q}) = 1.$$

In the second fit, charged current lepton universality is imposed and in the third fit, the W^+W^- cross-section is determined assuming Standard Model branching fractions. The results are summarised in Table 6.

Selected as	Expected signal	Expected back.	Total	Observed
$W^+W^- \to e^+\nu_e e^-\bar{\nu}_e$	8.6 ± 0.4	0.2 ± 0.4	8.8 ± 0.6	12
$W^+W^- \to e^+\nu_e \mu^-\bar{\nu}_\mu$	17.5 ± 0.6	0.2 ± 0.1	17.8 ± 0.6	11
$W^+W^- \to e^+\nu_e \tau^-\bar{\nu}_\tau$	16.7 ± 0.6	1.0 ± 1.0	17.6 ± 1.6	20
$W^+W^- \to \mu^+\nu_\mu \mu^-\bar{\nu}_\mu$	9.3 ± 0.3	1.4 ± 1.0	10.7 ± 1.0	13
$W^+W^- \to \mu^+\nu_\mu \tau^-\bar{\nu}_\tau$	14.6 ± 0.6	1.1 ± 1.0	15.7 ± 1.2	15
$W^+W^- \to \tau^+\nu_\tau \tau^-\bar{\nu}_\tau$	7.4 ± 0.4	0.8 ± 0.6	8.2 ± 0.7	7
$W^+W^- \to q\bar{q}e\bar{\nu}_e$	118.4 ± 2.8	11.3 ± 2.3	129.8 ± 3.6	140
$W^+W^- \to q\bar{q}\mu\bar{\nu}_\mu$	119.8 ± 2.7	3.4 ± 0.5	123.2 ± 2.8	120
$W^+W^- \to q\bar{q}\tau\bar{\nu}_\tau$	99.1 ± 3.0	19.2 ± 1.6	118.2 ± 3.3	101
$W^+W^- \to q\bar{q}q\bar{q}$	347.1 ± 8.3	95.5 ± 9.2	442.6 ± 12.4	438
Combined	758.4 ± 16.5	134.3 ± 9.6	892.7 ± 19.2	877

Table 5: Observed numbers of candidate events in each W^+W^- decay channel for an integrated luminosity of $(57.21 \pm 0.25)\ \text{pb}^{-1}$ at (182.68 ± 0.05) GeV together with expected numbers of signal and background events, assuming M_W=80.40 $\pm$ 0.09 GeV/c^2. The predicted numbers of signal events include systematic uncertainties from the efficiency, luminosity, beam energy, W^+W^- cross-section and M_W, while the background estimates include selection and luminosity uncertainties. The errors on the combined numbers account for correlations.

The hadronic branching fraction can be interpreted as a measurement of the sum of the squares of the six elements of the CKM mixing matrix, $|V_{ij}|$, which do not involve the top quark [1]:

$$\frac{\text{Br}(q\bar{q})}{(1 - \text{Br}(q\bar{q}))} = \left(1 + \frac{\alpha_s(M_W)}{\pi}\right) \sum_{i=u,c;\,j=d,s,b} |V_{ij}|^2,$$

Fitted parameter 183 GeV data	Fit assumptions :	Lepton universality	SM branching fractions
$\mathrm{Br}(\mathrm{W}\to \mathrm{e}\overline{\nu}_\mathrm{e})$	$0.121 \pm .010 \pm .003$		
$\mathrm{Br}(\mathrm{W}\to \mu\overline{\nu}_\mu)$	$0.107 \pm .009 \pm .003$		
$\mathrm{Br}(\mathrm{W}\to \tau\overline{\nu}_\tau)$	$0.094 \pm .011 \pm .003$		
$\mathrm{Br}(\mathrm{W}\to \overline{\ell}\nu_\ell)$		$0.108 \pm .004 \pm .002$	
$\mathrm{Br}(\mathrm{W}\to \mathrm{q}\overline{\mathrm{q}})$	$0.678 \pm .013 \pm .005$	$0.676 \pm .013 \pm .005$	
$\sigma_{\mathrm{WW}}(183\ \mathrm{GeV})$ [pb]	$15.33 \pm 0.61 \pm 0.27$	$15.43 \pm 0.61 \pm 0.26$	$15.43 \pm 0.61 \pm 0.26$

Fitted parameter 161-183 GeV data	Fit assumptions :	Lepton universality
$\mathrm{Br}(\mathrm{W}\to \mathrm{e}\overline{\nu}_\mathrm{e})$	$0.117 \pm .009 \pm .002$	
$\mathrm{Br}(\mathrm{W}\to \mu\overline{\nu}_\mu)$	$0.102 \pm .008 \pm .002$	
$\mathrm{Br}(\mathrm{W}\to \tau\overline{\nu}_\tau)$	$0.101 \pm .010 \pm .003$	
$\mathrm{Br}(\mathrm{W}\to \overline{\ell}\nu_\ell)$		$0.107 \pm .004 \pm .002$
$\mathrm{Br}(\mathrm{W}\to \mathrm{q}\overline{\mathrm{q}})$	$0.680 \pm .012 \pm .005$	$0.679 \pm .012 \pm .005$

Table 6: Summary of cross-section and branching fraction results from the 183 GeV data and the branching fraction results from the combination of the 161 GeV, 172 GeV and 183 GeV data. The results from three different fits described in the text are shown. The correlations between the branching fraction measurements from the fits without the assumption of lepton universality are less than 27%.

where $\alpha_s(M_\mathrm{W})$ is taken to be 0.120 ± 0.005. The branching fraction $\mathrm{Br}(\mathrm{W}\to \mathrm{q}\overline{\mathrm{q}})$ from the 161 – 183 GeV data obtained from the fit assuming lepton universality yields,

$$\sum_{i=\mathrm{u,c};\, j=\mathrm{d,s,b}} |\mathrm{V_{ij}}|^2 \quad = \quad 2.04 \pm 0.11 \pm 0.05.$$

This is consistent with a value of 2 which is expected from unitarity. Using the experimental knowledge [39] of the sum, $|\mathrm{V_{ud}}|^2+|\mathrm{V_{us}}|^2+|\mathrm{V_{ub}}|^2+|\mathrm{V_{cd}}|^2+|\mathrm{V_{cb}}|^2 = 1.05\pm 0.01$, the above result can be interpreted as a measure of $|\mathrm{V_{cs}}|$, which is the least well determined of these elements:

$$|\mathrm{V_{cs}}| \quad = \quad 0.99 \pm 0.06 \pm 0.02.$$

The measured $\mathrm{W^+W^-}$ production cross-section at $\sqrt{s} = 182.68$ GeV is shown in Figure 2 together with the recent OPAL measurements of σ_{WW} at $\sqrt{s} = 161.3$ GeV [40] and at $\sqrt{s} = 172.1$ GeV [28]. Figure 2 also shows the GENTLE prediction which is in excellent agreement with the data. On the other hand, the cross-section calculated without the contribution of the WWZ vertex, corresponding to anomalous couplings Δg_1^z=–1 and $\Delta\kappa_\mathrm{z}$=–1 (dashed line in Figure 2) fails to describe the data.

4.2 TGC analysis using the cross-section

A quantitative study of TGCs from the W-pair event yield is performed by comparing the numbers of observed events in each of the three event selection channels with the expected number which is parametrised as a second-order polynomial in the TGCs. This parametrisation is based on the linear dependence of the triple gauge vertex Lagrangian on the TGCs, corresponding to a second-order polynomial dependence of the cross-section. The polynomial coefficients are calculated from the expected cross-section in the presence of anomalous couplings determined with GENTLE and the slight dependence of our selection efficiency on the TGCs is obtained from the EXCALIBUR Monte Carlo samples. The Standard Model values for the W branching fractions are used. The background, which originates predominantly from $Z^0/\gamma \rightarrow q\overline{q}$ events, is assumed to be independent of the TGCs.

The probability to observe the measured number of candidates, given the expected value, is calculated using a Poisson distribution. The product of the three probability distributions corresponding to the three event selection channels is taken as the cross-section likelihood function.

The following sources of systematic uncertainty on the expected number of events are considered.

- The theoretical uncertainty in the expected cross-section which is obtained by comparing the cross-sections obtained from the GENTLE and EXCALIBUR programs. This uncertainty depends on the anomalous couplings and has a typical size of 2%.
- The small effect of the uncertainties in the W mass from the Tevatron measurement, (80.40 ± 0.09) GeV/c^2 [17], and the LEP centre-of-mass energy, (182.68 ± 0.05) GeV, on the total cross-section (less than 0.1% each).
- The uncertainties in the selection efficiencies and accepted background cross-sections, as listed in Tables 2 and 4.
- The uncertainty in the luminosity, of 0.5%.

The systematic uncertainties are incorporated into the TGC fit by allowing the expected numbers of signal and background events to vary in the fit and constraining them to have a Gaussian distribution around their expected values with their systematic errors taken as the width of the distributions. The systematic uncertainties, excluding those on efficiency and background, are assumed to be correlated between the three different event selections.

Data from lower centre-of-mass energies are included assuming all systematic errors to be fully correlated between energies. The corresponding $\log L$ curves are used in combination with the results of the angular distribution analyses which are described in the following sections. The full set of results are then presented in Figure 12, where the cross section contributions are shown as dotted lines.

5 Analysis of the $W^+W^- \rightarrow q\overline{q}\overline{\ell}\nu_\ell$ angular distributions

The analysis of the $W^+W^- \rightarrow q\overline{q}\overline{\ell}\nu_\ell$ channel is performed in three different ways using optimal observables (OO), a binned maximum likelihood (BML) fit, and the spin density matrix (SDM).

These three methods will be described in the following sub-sections. All methods use the same selection and reconstruction procedure. The selection procedure starts from the event sample used for the total cross-section analysis with further cuts imposed in order to assure a reliable reconstruction of the event kinematics and to reduce further the background.

5.1 Event selection and reconstruction

The selection of $\mathrm{q\overline{q}e\overline{\nu}_e}$ and $\mathrm{q\overline{q}}\mu\overline{\nu}_\mu$ events for the total cross-section analysis results in a single track being identified as the most likely lepton candidate. The electron momentum vector is reconstructed by the tracking detectors and the energy is measured in the electromagnetic calorimeters. In the case of muons, the momentum measured using the tracking detectors is used. The remaining tracks and calorimeter clusters in the event are grouped into two jets using the Durham $k_\perp$ algorithm [32]. The total energy and momentum of each of the jets are calculated with the method described in [33]. A one-constraint kinematic fit is then performed on the events, requiring energy-momentum conservation and allowing for a massless neutrino. Events are accepted if this fit converges with a probability larger than 0.001. This cut rejects about 2% of the signal events and 10% of the background.

To improve the resolution in the angular observables used for the TGC analysis, we perform a further kinematic fit with three constraints requiring energy-momentum conservation and the fitted masses of both the hadronic and the leptonic systems to be constrained to the average Tevatron W mass, M_W=80.40 GeV/c^2 [17], within the W width[10]. We demand that the kinematic fit converges with a probability larger than 0.001. For the $\approx$3% of events which fail at this point we revert to using the results of the fit without the W mass constraint.

The selection of the $\mathrm{q\overline{q}}\tau\overline{\nu}_\tau$ events results in the identification of the most likely tau decay candidate classified as an electron, muon, one-prong hadronic or three-prong hadronic decay. The remaining tracks and calorimeter clusters in the event are grouped into two jets as described above. However, these events cannot be reconstructed in the same way since there is more than one unobserved neutrino. Nevertheless, as the tau is highly relativistic, its flight direction can be approximated by the direction of its charged decay products, leaving us with four unknown quantities, the tau energy and the prompt neutrino three-momentum vector. A one-constraint kinematic fit is performed on the event requiring energy-momentum conservation and equality between the masses of the hadronic and leptonic systems. This fit is required to converge with a probability larger than 0.001. In addition, the angle between the two jets in the hadronic system, θ_{jj}, is required to satisfy $\cos\theta_{jj} < -0.2$, and the angle between the tau and the closest jet is required to exceed 20^o. These cuts reject 20% of the signal and 42% of the background. Furthermore, these cuts suppress those $\mathrm{q\overline{q}}\tau\overline{\nu}_\tau$ events which are correctly identified as belonging to this decay channel but where the tau decay products are not identified correctly, leading to an incorrect estimate of the tau flight direction or its charge. The fraction of such events in the $\mathrm{q\overline{q}}\tau\overline{\nu}_\tau$ sample is reduced by these cuts from 13% to 8.5%.

After these cuts, 324 $\mathrm{q\overline{q}}\overline{\ell}\nu_\ell$ candidates remain (135 $\mathrm{q\overline{q}e\overline{\nu}_e}$, 116 $\mathrm{q\overline{q}}\mu\overline{\nu}_\mu$ and 73 $\mathrm{q\overline{q}}\tau\overline{\nu}_\tau$). The

[10] The W mass distribution is treated as a Gaussian in the kinematic fit. However, in order to simulate the expected Breit-Wigner form of the W mass spectrum, the variance of the Gaussian is updated at each iteration of the kinematic fit in such a way that the probabilities of observing the current fitted W mass are equal whether calculated using the Gaussian distribution or using a Breit-Wigner.

remaining background fraction, assuming Standard Model cross-sections for signal and background processes, is 6.2%, not including cross-migration between the three lepton channels. The background sources are: four-fermion processes after subtracting the contribution of the CC03 diagrams (3.8%), $Z^0/\gamma \rightarrow q\overline{q}$ (1.9%), $W^+W^- \rightarrow q\overline{q}q\overline{q}$ and $\overline{\ell}\nu_\ell\ell'\overline{\nu}_{\ell'}$ (0.3%) and two-photon reactions (0.2%).

In the reconstruction of the $q\overline{q}\ell\nu_\ell$ events we obtain $\cos\theta_W$ by summing the kinematically fitted four-momenta of the two jets. The decay angles of the leptonically decaying W are obtained from the charged lepton four-momentum, after boosting back to the parent W rest frame. In the hadronically decaying W we are left with a twofold ambiguity in assigning the jets to the quark and antiquark. This ambiguity is taken into account in the analyses described below.

In Figure 3 (a-e) we show the distributions of all the five angles obtained from the combined $q\overline{q}\ell\nu_\ell$ event sample, and the expected distributions for $\Delta g_1^z = \pm1$ and 0. These expected distributions are obtained from fully simulated Monte Carlo event samples generated with EXCALIBUR, normalised to the number of events observed in the data. Sensitivity to TGC is observed mainly for $\cos\theta_W$. The contribution of $\cos\theta_\ell^*$, ϕ_ℓ^*, $\cos\theta_{\rm jet}^*$ and $\phi_{\rm jet}^*$ to the overall sensitivity enters mainly through their correlations with $\cos\theta_W$.

5.2 The Optimal Observable (OO) analysis

The concept of optimal observables [41] is used to project the five kinematic variables of each event onto a single observable. It has been shown that for a differential cross-section which is linear in the parameter to be determined, the sensitivity of the optimal observable is the same as for a multi-dimensional maximum likelihood fit. The W-pair differential cross-section is, however, a second-order polynomial in the couplings, thus leading to a loss of sensitivity when constructing the optimal observable without the quadratic term. Nevertheless, in the case where the deviations of the couplings from zero are small, the quadratic terms are suppressed and the loss in sensitivity is far outweighed by the great advantage of a parametrisation in only one dimension. This method also allows usage of all the available kinematic information from the event, whereas in other methods (see the next sub-sections) some part of the information is lost due to computational limitations.

The optimal observable for measuring any particular TGC parameter, α, is constructed for each event i with the set of phase-space variables $\Omega = (\cos\theta_W, \cos\theta_\ell^*, \phi_\ell^*, \cos\theta_{\rm jet}^*, \phi_{\rm jet}^*)$ by differentiating the differential cross-section for the event, $\sigma_i(\alpha) \equiv d\sigma(\Omega,\alpha)/d\Omega)|_{(\Omega=\Omega_i)}$, with respect to the parameter α evaluated at the Standard Model value, α=0, and normalising to the Standard Model cross-section,

$$\mathcal{O}_i = \frac{1}{\sigma_i^{\rm SM}}\frac{d\sigma_i(\alpha)}{d\alpha}|_{(\alpha=0)}.$$

The differential cross-section used here is the Born cross-section, taking into account the twofold ambiguity in the definition of the measured $\cos\theta_{\rm jet}^*$ and $\phi_{\rm jet}^*$.

Figure 3(f) shows the distribution of the optimal observable corresponding to Δg_1^z, along with the predictions corresponding to the Standard Model and to $\Delta g_1^z = \pm1$, as obtained from corresponding Monte Carlo samples. Similar distributions are obtained for the optimal observables corresponding to $\Delta\kappa_\gamma$ and λ.

A binned maximum likelihood fit of the expected optimal observable distributions to the data is performed to extract each coupling, assuming the other two couplings to have Standard Model values. The expected optimal observable distributions for various couplings are derived from Monte Carlo events and normalised to the number of events in the data in order to exclude any information from the overall production rate in this part of the analysis. To obtain the optimal observable distribution at intermediate parameter values, a reweighting technique is applied to sets of Monte Carlo events generated with different couplings using a Born-level differential cross-section but taking into account ISR effects.

The method is tested with about 350 Standard Model and 200 non-Standard Model Monte Carlo subsamples, each corresponding to the collected luminosity. Summing up the $\log L$ curves from the different subsamples corresponding to the same coupling gives results which are consistent with the coupling value used in the Monte Carlo generation. Unfortunately, for the Standard Model subsamples the $\log L$ curves corresponding to $\Delta\kappa_\gamma$ tend to have two minima, one close to the generated value, $\Delta\kappa_\gamma$=0, and the second around $\Delta\kappa_\gamma$=2.5. The second minimum is due to the fact that, for example, the normalised differential cross-section for $\Delta\kappa_\gamma$=2.5 is more similar to the Standard Model than the one for $\Delta\kappa_\gamma$=1. In about 18% of the cases the wrong minimum is the deepest one. However, the cross-section information already excludes a value around 2.5 for $\Delta\kappa_\gamma$ (see Figure 12). Therefore, the minimum at that point can be disregarded. A similar problem occurs in 3% (7%) of the Standard Model subsamples also for Δg_1^z (λ) where the constraint from the cross-section information is even more stringent, so it is handled in the same way.

The error interval is defined in the usual way, as the region where the $\log L$ function is higher than its minimum by no more than 0.5. To test the reliability of this error estimate, the fraction of subsamples where the correct value is within the error interval is calculated. The error estimate is considered to be reliable if the calculated fraction is consistent with 68%, which is the case for all couplings.

Performing the fit to the 183 GeV data, we obtain the results quoted in the first row of Table 8. The statistical errors obtained from the fit are consistent with the expected values which are estimated from the distribution of the Monte Carlo subsample fit results.

Biases introduced by uncertainties in the simulation of the detector acceptance are checked by removing events in phase-space regions where the efficiency changes rapidly. Cuts on the polar angles of the charged lepton and the neutrino, on the angle between the lepton and the nearest jet, as well as a cut on the lepton energy, were introduced. Furthermore the range of the OO-values that are considered in the fit is changed by approximately $\pm$10%. The variations of the fit result due to these changes fall within the statistical fluctuations determined using many Monte Carlo subsamples with the size of the data sample.

The effect of Monte Carlo statistics is studied by allowing the expected number of events in each bin of the optimal observable distribution to vary around its central value within its error according to a Gaussian distribution. This effect is found to be negligible.

Additional systematic uncertainties are studied due to the following effects.

a) For quark jets in the Monte Carlo samples, the resolutions of the three jet parameters (energy, $\cos\theta, \phi$) are varied by 10%, and the energy scale is shifted by 0.5% to account for systematic uncertainties in the modelling of the jet reconstruction. The size of the variations is determined from extensive studies of back-to-back jets at LEP Z^0 energies. A possible systematic shift in the reconstructed direction of the W boson has been estimated using radiative $Z^0/\gamma \to q\overline{q}$ events. The shift in $|\cos\theta_W|$ was found to be less than 0.01 [11]. The same reconstruction uncertainties are assumed also for the τ jets in $q\overline{q}\tau\overline{\nu}_\tau$ events.

b) Uncertainties in the fragmentation model are studied using a Monte Carlo sample generated with HERWIG rather than PYTHIA.

c) Differences between Monte Carlo generators not related to fragmentation are investigated by replacing the EXCALIBUR reference sample by KORALW. This latter generator also uses the JETSET fragmentation scheme but has a different treatment of ISR and simulates correctly the τ helicity effects.

d) Systematic effects arising from the simulation of the $Z^0/\gamma \to q\overline{q}$ background are taken into account by replacing PYTHIA with HERWIG. The two-photon background is removed to test its impact on the measurement. The four-fermion processes from $e^+e^- \to We\overline{\nu}_e$, $e^+e^- \to Z^0e^+e^-$ and $e^+e^- \to Z^0Z^0$ are added as background to the CC03 diagrams, neglecting interference. The justification for this simplification is verified by using a fully simulated four-fermion Monte Carlo (EXCALIBUR) as the reference sample. In addition, subsamples of fully simulated four-fermion Monte Carlo events have been fitted and no bias was found. To test the Monte Carlo generators, samples of KORALW and `grc4f` generated with the CC03 W-pair diagrams according to the Standard Model are used as test samples and all the TGC results are found to be consistent with zero.

Source		Error on parameter		
		$\Delta\kappa_\gamma$	Δg_1^z	λ
a)	Jet reconstruction	.114	.029	.033
b)	Fragmentation	.088	.012	.012
c)	MC generator	.049	.003	.011
d)	Background	.093	.029	.010
	Combined	.178	.043	.038

Table 7: Contributions to the systematic uncertainties in the determination of the TGC parameters in the OO analysis for the $W^+W^- \to q\overline{q}\ell\nu_\ell$ angular distributions of the 183 GeV data.

Table 7 summarises the various components of the systematic errors. These are incorporated into the $\log L$ functions by convolving their distributions, assumed to be Gaussian, with the likelihood functions. The corrected likelihood functions resulting from this convolution are used to obtain new values for the TGC parameters with modified errors which include the systematic uncertainties. The new TGC values may differ from those obtained before the convolution due to the asymmetric nature of the likelihood function. The results are listed in Table 8.

5.3 The Binned Maximum Likelihood (BML) analysis

The BML analysis has been used to analyse our previous data taken at 161 GeV and 172 GeV and is fully described in [9, 11]. The finite statistics of the data and Monte Carlo samples limits the number of kinematic observables which can be used to three. The most sensitive ones, namely $\cos\theta_{\mathrm{W}}$, $\cos\theta^*_\ell$ and ϕ^*_ℓ are chosen[11]. The expected three-dimensional distribution of these observables as a function of the TGCs is fitted to the corresponding distribution of the data. The expected distribution is obtained from MC events generated according to the Standard Model with the CC03 diagrams. These events are reweighted to correspond to any other TGC value. The reweighting procedure uses very large statistics MC samples at the generator level, generated with ten different sets of TGC values and used to produce ten basis distributions. Since the differential cross-section is a second-order polynomial in the TGCs (see section 4.2 above), the distribution corresponding to any other set of TGC values can be obtained by a proper linear combination of the ten basis distributions.

This procedure accounts for the effects of efficiency, resolution and background from other $\mathrm{W^+W^-}$ decay channels. To account also for non-$\mathrm{W^+W^-}$ background, the contribution of background sources which do not depend on the TGCs, namely $\mathrm{Z^0}/\gamma \to \mathrm{q\overline{q}}$, $\mathrm{q\overline{q}e^+e^-}$ and two-photon reactions, is added to the expected distribution used in the fit. The distributions from these sources are obtained from corresponding Monte Carlo samples. Background from other four-fermion diagrams which is TGC-dependent is neglected at this stage, and biases caused by this neglect are evaluated by performing the fit on four-fermion MC events taken as a test sample. These biases are subtracted from our fit results.

The expected distribution is normalised to the number of events observed in the data in order not to incorporate any information from the overall production rate in this part of the analysis. The probability for observing the number of events seen in each bin is calculated using Poisson statistics. The statistical fluctuations in the Monte Carlo are taken into account using the method of reference [42]. Consequently, the errors obtained from the fit include both data and Monte Carlo statistics.

Detector level MC samples generated with different TGCs are used to verify that the BML fit method introduces no bias. The reliability of the statistical errors obtained from the fit is checked with many Monte Carlo subsamples, in the way described in section 5.2. A problem occurs only for $\Delta\kappa_\gamma$ where the fraction of subsamples with the correct TGC value within the error interval falls below 68%. It is found that dividing the $\log L$ function by a correction factor of 1.21 increases the error interval in such a way that this fraction reaches 68%. This correction factor is then applied to the $\log L$ function extracted from the data. The statistical errors obtained in this way are also consistent with the expected values which are listed in Table 8.

The systematic errors are evaluated and incorporated into the $\log L$ functions in a similar way as for the OO method. The results are consistent with those of the OO method.

5.4 The Spin Density Matrix (SDM) analysis

Spin density matrix elements are observables directly related to the polarisation of the W bosons [1, 43]. Additional insight into the underlying physics may be gained from these spin-related observables, and the relative production of various helicity states of the W bosons can be measured. Comparing the spin density matrix elements with the theoretical predictions

[11] The observables $\cos\theta^*_{\mathrm{jet}}$ and ϕ^*_{jet} have smaller sensitivities due to their twofold ambiguity.

allows a model-independent test of the TGCs. If deviations were detected, this method would give information on the structure of the anomalous couplings.

Spin density matrix elements are normalised products of the helicity amplitudes $\mathcal{F}^{(\lambda)}_{\tau_-\tau_+}(\cos\theta_{\mathrm{W}})$, where τ_- and τ_+ are the helicity states of the W^- and W^+ boson, respectively, and λ denotes the spin of the $\mathrm{e}^+\mathrm{e}^-$ system. The two-particle joint density matrix elements are defined according to

$$\rho_{\tau_-\tau'_-\tau_+\tau'_+}(\cos\theta_{\mathrm{W}}) = \frac{\sum_\lambda \mathcal{F}^{(\lambda)}_{\tau_-\tau_+}(\mathcal{F}^{(\lambda)}_{\tau'_-\tau'_+})^*}{\sum_{\lambda\tau_+\tau_-}|\mathcal{F}^{(\lambda)}_{\tau_-\tau_+}|^2}.$$

Due to limited statistics in the analysis described here the single-W spin density matrix elements $\rho_{\tau\tau'}$ are used. The spin density matrix of the W^- boson, for example, is obtained from the two-particle joint density matrix elements by the relation

$$\rho^{\mathrm{W}^-}_{\tau_-\tau'_-}(\cos\theta_{\mathrm{W}}) = \sum_{\tau_+}\rho_{\tau_-\tau'_-\tau_+\tau_+}(\cos\theta_{\mathrm{W}}).$$

The matrix $\rho_{\tau\tau'}$ is hermitian, thus having six independent matrix elements. The diagonal elements $\rho_{\tau\tau}$ of the spin density matrix are real and can be interpreted as the probability to produce a W boson with helicity τ. The off-diagonal elements are complex in general, but for CP-conserving theories the imaginary parts vanish.

The spin density matrix elements are extracted with the help of projection operators [1,43]. These operators reflect the standard $V-A$ couplings of the fermions to the W boson in the W decay. The single-W spin density matrix elements $\rho_{\tau\tau'}$ can be extracted using the threefold differential cross-section $d\sigma/d\cos\theta_{\mathrm{W}}d\cos\theta^* d\phi^*$ from the relation

$$\rho^{\mathrm{W}_1}_{\tau\tau'}(\cos\theta_{\mathrm{W}})\frac{d\sigma(\mathrm{e}^+\mathrm{e}^-\to\mathrm{W}_1\mathrm{W}_2)}{d\cos\theta_{\mathrm{W}}} = \frac{1}{\mathrm{Br}_{\mathrm{W}_1\to\mathrm{f\bar{f}}}}\int\frac{d\sigma(\mathrm{e}^+\mathrm{e}^-\to\mathrm{W}_2\mathrm{f\bar{f}})}{d\cos\theta_{\mathrm{W}}d\cos\theta^*_1 d\phi^*_1}\Lambda_{\tau\tau'}(\theta^*_1,\phi^*_1)d\cos\theta^*_1 d\phi^*_1. \quad (2)$$

Here $\Lambda_{\tau\tau'}$ is the suitable projection operator for extracting the spin density matrix element $\rho_{\tau\tau'}$ and $\mathrm{Br}_{\mathrm{W}_1\to\mathrm{f\bar{f}}}$ is the branching ratio for the decay of the W boson considered. Expressions for the projectors can be found in [43]. Experimentally, equation 2 corresponds to

$$\rho_{\tau\tau'}(\cos\theta_{\mathrm{W}}) = \frac{1}{N}\sum_{i=1}^{N}\Lambda_{\tau\tau'}(\cos\theta^*{}_i,\phi^*{}_i)$$

where N is the number of events and $\Lambda = \Lambda(\cos\theta^*{}_i,\phi^*{}_i)$ is the value of the projection operator of event i. The spin density matrix elements are extracted in bins of $\cos\theta_{\mathrm{W}}$.

For the leptonically decaying W, the full information about the W decay angles is accessible and the matrix elements can be directly extracted according to (2). For hadronic decays of the W boson where the quark cannot be distinguished from the antiquark, only the folded angular distributions of $\cos\theta^*$ and ϕ^* are directly available. These folded distributions can be identified only with the symmetric[12] part of the angular distributions [3], whereas no information about the antisymmetric part is accessible. The following symmetric (combinations of) spin density matrix elements can be extracted from the folded angular distribution by using the symmetric part of the projection operators only:

$$\rho_{++}+\rho_{--},\quad \rho_{00},\quad \mathrm{Re}(\rho_{+-}),\quad \mathrm{Im}(\rho_{+-}),\quad \mathrm{Re}(\rho_{+0}-\rho_{-0}),\quad \mathrm{Im}(\rho_{+0}+\rho_{-0}).$$

[12] Symmetric/antisymmetric under the transformation $\cos\theta^*\to-\cos\theta^*$, $\phi^*\to\phi^*+\pi$

The correlations between the single-W density matrix elements are calculated analytically.

In order to compare the density matrix elements extracted from data with the theoretical predictions, the data have to be corrected for experimental effects, like selection efficiency, acceptance, angular resolution and the effect of ISR. A simple approach, based on a Standard Model Monte Carlo, is performed. First the expected background, taken from Monte Carlo, is subtracted on a statistical basis. Subsequently the data are corrected by multiplying the three-dimensional angular distribution by a correction function which is given by the ratio of the angular distributions for the reconstructed angles in the selected events and the generator level distributions of all events. The effect of ISR is approximately accounted for by reducing the centre-of-mass energy by the mean energy of initial state photons, $\langle E_{\mathrm{ISR}} \rangle = 1.6$ GeV, as determined from Monte Carlo.

Distributions of the spin density matrix elements of the leptonically decaying W and the hadronically decaying W are shown in Figures 4 and 5. Overlaid are the analytical predictions as expected in the Standard Model. The errors are statistical. The systematic errors are estimated to be less than 10% of the statistical errors. This is verified by replacing the Standard Model Monte Carlo sample used for the correction of detector effects with samples generated with $\Delta g_1^z = \pm 1$ values which are far outside the allowed region obtained in our fit (see below).

The measurements of the W-pair cross-section, the $\cos\theta_{\mathrm{W}}$ distribution and the spin density matrices can be combined to give a measurement of the semi-inclusive differential cross-sections, to produce a transversely polarised W, $\mathrm{e^+e^-} \to \mathrm{W_T W}$, or a longitudinally polarised W, $\mathrm{e^+e^-} \to \mathrm{W_L W}$, where in either case the second W can have arbitrary helicity. For this purpose, the raw $\cos\theta_{\mathrm{W}}$ distribution, plotted in Figure 3(a), is corrected for detector effects by subtracting the background and multiplying by a correction function for efficiency and resolution obtained from Standard Model Monte Carlo. The systematic error associated with this correction is estimated in the same way as for the OO analysis. In addition, as was done for the spin density matrix elements, the Standard Model Monte Carlo sample used for the correction of detector effects is replaced by samples generated with $\Delta g_1^z = \pm 1$. The corrected $\cos\theta_{\mathrm{W}}$ distribution is multiplied by our measured total cross-section and the corresponding spin density matrix elements after combining their values from the leptonic and hadronic decays. The resulting differential cross-sections, plotted in Figure 6, are seen to be consistent with the Standard Model expectations. Integrating over these cross-sections, the overall fraction of longitudinally polarised W bosons is determined to be $0.242 \pm 0.091 \pm 0.023$, where the systematic error is dominated by uncertainties in the jet and tau resolutions (0.017) and MC generator (0.015). The expected value for this fraction is 0.272 (0.392, 0.405) for the Standard Model (Δg_1^z=+1, −1).

The spin density matrix elements can be used to extract the TGCs by comparing them, before the various corrections, to those expected from Monte Carlo events for different TGC values. This is done with a reweighting technique, taking into account all experimental effects. The W production angle and the spin density matrix elements of both W bosons are used in the fit. We obtain results consistent with those from the OO method.

5.5 Summary of the $q\overline{q}\ell\overline{\nu}_\ell$ analyses

All three methods described above give consistent results for the 183 GeV data. The OO results are chosen to be combined with the results of the other channels and the cross-section result since this method is expected to give the best sensitivity, as can be seen from the expected errors listed in Table 8.

Level of results	$\Delta\kappa_\gamma$	Δg_1^z	λ
Without systematics	$-0.21^{+0.61}_{-0.45}$	0.00 ± 0.14	-0.19 ± 0.15
Expected errors, OO method	± 0.46	± 0.13	± 0.14
Expected errors, BML method	± 0.56	± 0.16	± 0.19
Expected errors, SDM method	± 0.50	± 0.14	± 0.16
Including systematics	$-0.18^{+0.77}_{-0.56}$	0.00 ± 0.16	-0.19 ± 0.16
Including 161/172 GeV angular data	$-0.08^{+0.71}_{-0.54}$	-0.01 ± 0.15	-0.16 ± 0.16
Including cross-section	$0.04^{+0.67}_{-0.44}$	-0.01 ± 0.14	$-0.14^{+0.15}_{-0.14}$

Table 8: Measured values of the TGC parameters using the $q\overline{q}\ell\overline{\nu}_\ell$ event selection analysed with the OO method, with and without taking into account the systematic uncertainty. We also list the results after combining with our 161 and 172 GeV data and after combining with the cross-section information of $q\overline{q}\ell\overline{\nu}_\ell$ data from all centre-of-mass energies. The expected statistical errors obtained from Monte Carlo studies are listed for all three analysis methods.

Although our method of OO analysis using the optimal observable distribution is preferred for single parameter fits, it is less well suited to a fit of two or three TGC parameters. In this case, two- or three-dimensional distributions of the optimal observables corresponding to the different TGC combinations would be required, and it is simpler to fit the angular variables directly, using the BML method.

The 183 GeV results are combined with our 161 GeV and 172 GeV results [11]. In the 161 GeV analysis [9] only the parameter $\alpha_{W\phi}$ has been analysed. Therefore, this analysis is extended here using the same (BML) method to include the three parameters $\Delta\kappa_\gamma$, Δg_1^z and λ, along with the two-dimensional and three-dimensional fits. All the tests and the systematic studies are done in the same way as for the 183 GeV BML analysis. The correlation between the systematic errors of the $q\overline{q}\ell\overline{\nu}_\ell$ results from the three centre-of-mass energies is neglected since, using the BML method, it is found to affect the results by no more than 10% of their statistical errors.

Table 8 summarises the $q\overline{q}\ell\overline{\nu}_\ell$ results from the 183 GeV data, the results obtained after combining the 161 and 172 GeV data, and the combined $q\overline{q}\ell\overline{\nu}_\ell$ results obtained after adding also the cross-section information for that channel from all centre-of-mass energies. The $\log L$ curves corresponding to the combined $q\overline{q}\ell\overline{\nu}_\ell$ results are shown in Figure 11. The correlation between the systematic errors of the angular distributions and the cross-section, mainly due to the uncertainty in the background level, is neglected as it affects the results by less than 1% of their statistical errors.

6 Analysis of the $\mathrm{W^+W^-} \rightarrow \mathrm{q\bar{q}q\bar{q}}$ angular distributions

The analysis of the $\mathrm{W^+W^-} \rightarrow \mathrm{q\bar{q}q\bar{q}}$ channel is performed on both the 172 GeV and the 183 GeV data. It uses the same event samples as the cross-section analyses (see section 3.3 and ref. [11]).

6.1 Event selection and reconstruction

Using the Durham $k_\perp$ algorithm [32], each selected event is forced into 4 jets, whose energies are corrected for the double counting of charged track momenta and calorimeter energies [33]. To improve the resolution on the jet four-momentum we perform a kinematic fit requiring energy-momentum conservation and equality of the masses of the two W candidates (5-C fit). The event reconstruction is complicated by the ambiguity in the choice of the correct di-jet combination and uncertainties in the determination of the W charge. The latter is assigned by comparing the sum of the charges of the two jets coming from the same W candidate. Each W charge is defined as:

$$Q_{W_1} = \frac{N_i + N_j}{\sum_{m=1}^{4} D_m}, \qquad Q_{W_2} = \frac{N_k + N_l}{\sum_{m=1}^{4} D_m},$$

where jets i and j belong to $\mathrm{W_1}$, jets k and l belong to $\mathrm{W_2}$, and N_{jet} and D_{jet} are given by:

$$N_{jet} = \sum_{i=1}^{N} q_i |p_{i||}|^{0.5}, \qquad D_{jet} = \sum_{i=1}^{N} |p_{i||}|^{0.5}$$

where q_i is the charge of the i^{th} track, $p_{i||}$ is the projection of its momentum along the jet axis and N is the total number of tracks in the jet.

One di-jet combination is chosen out of the three possible ones by a likelihood algorithm. The input variables to the likelihood are the di-jet invariant masses, obtained by a kinematic fit requiring energy and momentum conservation (4-C fit), the charges of the two W candidates, and the probabilities of the 5-C kinematic fits. Once a jet combination is chosen, the $\mathrm{W^-}$ is defined as the di-jet whose charge is more negative. According to the Monte Carlo simulation, these choices correspond to a probability of selecting the correct di-jet combination of about 78% (82%) at 183 (172) GeV, and to a probability of correct assignment of the W charge, once the correct pairing has been chosen, of about 76%. Both probabilities show a few percent dependence on the value of an eventual anomalous TGC. Incorrect jet pairing and wrong determination of the W charge decrease the sensitivity of the reconstructed $\cos\theta_\mathrm{W}$ distribution to possible TGCs. To increase the fraction of events correctly reconstructed, we apply further cuts on the value of the jet pairing likelihood, $L > 0.8$, and on the W charge separation, $|Q_{\mathrm{W}_1} - Q_{\mathrm{W}_2}| > 0.04$. The distributions of these variables, for the data collected at 183 GeV and for the corresponding Monte Carlo, are shown in Figure 7. The cut values are the result of a compromise between loss in efficiency and gain in sensitivity. After these cuts, the probability of correct pairing increases to 86% (87%) at 183 (172) GeV and the probability of correct determination of the W charge to 82%. The selection efficiency is reduced by about 40%, whereas the $Z^0/\gamma \to q\overline{q}$ background is reduced by 60% and 70% at 172 and 183 GeV respectively. At 172 GeV, 41 events survive all cuts out of the 59 initially selected, and 241 out of 438 events remain finally at 183 GeV. The $\cos\theta_W$ distributions obtained at both energies are shown in Figure 8 together with the distributions predicted by the Monte Carlo for different values of λ.

6.2 TGC analysis

Due to lack of separation between quarks and antiquarks, in $W^+W^- \to q\overline{q}q\overline{q}$ events most of the sensitivity to the TGCs is contained in the $\cos\theta_W$ distribution. A binned maximum likelihood method is thus used in this channel. The measured $\cos\theta_W$ distribution is divided into ten bins in the range [–1,1]. The expected cross-section in each bin i, σ_i, due to W^+W^- production is parametrised as a second-order polynomial in the analysed coupling. Monte Carlo reference histograms, including all effects of acceptance, resolution, incorrect jet pairing and incorrect determination of the W charge, are used to build the parametrisation. The contribution of the $Z^0/\gamma \to q\overline{q}$ background as obtained from the PYTHIA Monte Carlo is added to the W-pair expectation. To avoid any dependence on the overall production rate, the expected cross-section is normalised to the total number of candidates. The expected distribution is fitted to the data using a binned maximum likelihood method and assuming Poisson statistics. The result of the fits to $\Delta\kappa_\gamma$, Δg_1^z and λ as obtained from the 183 GeV data sample are given in the first row of Table 10 where the quoted errors are statistical only.

The reliability of the statistical error estimates is checked by performing the analysis on many subsamples of Monte Carlo events, each corresponding to the data luminosity. The r.m.s. values of the fit results corresponding to these subsamples are quoted in the second row of Table 10. These values are somewhat lower than the statistical errors coming from the fits to the data. However, the data statistical errors are still compatible with their expected values with probabilities above 5%, as obtained from the MC subsample study. As a further test, the fraction of subsamples where the correct TGC value turns out to be inside the error interval is checked and found to be consistent with 68%, as required.

The following sources of systematic errors are considered:

a) The effect of possible differences in the jet resolution between data and Monte Carlo is studied in the Monte Carlo by smearing and shifting the jet energies and directions in the same way as done for the $q\overline{q}\ell\nu_\ell$ analysis. The resulting changes caused to the measured TGCs are added in quadrature and taken as a systematic error.

b) Possible dependences on fragmentation models are studied by comparing the results of the fit to two Monte Carlo samples generated with PYTHIA. In the first sample, the JETSET [22] fragmentation model is implemented as for the reference Monte Carlo samples, whereas in the second it is replaced by HERWIG. The implementation of HERWIG mainly results in a higher probability of correct jet pairing and correct W charge with respect to JETSET. The statistics of the data are insufficient to discriminate between the two models. We assign as a systematic error for each coupling the difference we find in the results of the fits to the two Monte Carlo samples.

c) We study possible biases due to the choice of the Monte Carlo generator by repeating the fit to W^+W^- samples generated with PYTHIA, KORALW and `grc4f`.

d) A systematic error on the estimation of the background is determined by varying both its shape and normalisation. The shape predicted by PYTHIA is replaced by that predicted by HERWIG. The normalisation is varied by the background uncertainty as determined from the analysis of the cross-section. The feed-through from other W boson decay channels is less than 0.2% and is neglected. The effect of neglecting the contribution of four-fermion diagrams is studied by performing the analysis on various four-fermion Monte Carlo samples generated with EXCALIBUR and `grc4f`. The corresponding shifts on the fitted values of each TGC parameter are added in quadrature and taken as a systematic error.

e) Bose-Einstein correlations (BEC) between bosons originating from different W in the event might affect the measured W charge distribution. This effect is studied at 183 GeV with a PYTHIA Monte Carlo sample [44] where BEC have been implemented.

f) The measured W charge distribution might be affected also by colour reconnection. This effect is investigated at 183 GeV with Monte Carlo samples generated with PYTHIA, in two classes of reconnection models called type I and type II [45], and with ARIADNE [46].

g) Finally, a possible presence of biases in our analysis or fit method is checked by analysing Monte Carlo events generated with known values of the couplings, ranging from −2 to +2. As a consistency check we use large Monte Carlo samples. We also perform fits to many small Monte Carlo subsamples as mentioned above and examine the sum of their likelihood functions.

	Source	Error on parameter		
		$\Delta\kappa_\gamma$	Δg_1^z	λ
a)	Jet reconstruction	0.26	0.08	0.09
b)	Fragmentation	0.30	0.10	0.20
c)	MC generator	0.45	0.10	0.13
d)	Background	0.22	0.06	0.10
e)	BEC	0.07	0.04	0.02
f)	Colour reconnection	0.01	0.01	0.01
g)	Fit bias tests	0.20	0.08	0.09
	Combined	0.68	0.19	0.29

Table 9: Contributions to the systematic errors in the determination of the three TGC parameters for the $W^+W^- \to q\bar{q}q\bar{q}$ angular distribution analysis of the 183 GeV data.

The results of all these systematic studies for the 183 GeV data are summarised in Table 9. The systematic errors for the 172 GeV data are similar and are assumed to be fully correlated with those of the 183 GeV data. The combined systematic errors are convolved with the likelihood functions. The results for the 183 GeV data sample after convolving the systematic errors are listed in the third row of Table 10. After combining with the 172 GeV data, we obtain the results listed in the fourth row of Table 10. Finally, we combine also the results of the cross-section analysis in this channel, using the 161, 172 and 183 GeV data samples, yielding the results quoted in the last row of Table 10. The corresponding $\log L$ functions are plotted in Figure 11.

Level of results	$\Delta\kappa_\gamma$	Δg_1^z	λ
Without systematics	$1.15^{+1.28}_{-1.25}$	$0.68^{+0.91}_{-0.64}$	$0.76^{+0.78}_{-0.67}$
Expected errors	±1.13	±0.43	±0.52
Including systematics	$1.16^{+1.39}_{-1.34}$	$0.73^{+0.88}_{-0.72}$	$0.79^{+0.79}_{-0.78}$
Including 172 GeV data	$1.15^{+1.35}_{-1.36}$	$0.62^{+0.97}_{-0.62}$	$0.68^{+0.80}_{-0.68}$
Including cross-section	$0.85^{+0.68}_{-1.01}$	$0.24^{+0.24}_{-0.30}$	$0.30^{+0.28}_{-0.36}$

Table 10: Measured values of the three TGC parameters using the $q\overline{q}q\overline{q}$ event selection from the 183 GeV data, with and without taking into account the systematic uncertainties. The second row gives the expected statistical error from Monte Carlo studies. The fourth row shows the results after combining with the 172 GeV data, and in the last row we list the results after combining with the cross-section information of $q\overline{q}q\overline{q}$ data from the 161, 172 and 183 GeV centre-of-mass energies.

7 Analysis of the $W^+W^- \to \overline{\ell}\nu_\ell\ell'\overline{\nu}_{\ell'}$ angular distributions

In a $W^+W^- \to \overline{\ell}\nu_\ell\ell'\overline{\nu}_{\ell'}$ event, there are at least two undetected neutrinos. Fortunately, in the small-width, no-ISR approximation, the W production and decay angles can still be reconstructed from the measured charged lepton momenta, provided there are only two missing neutrinos – thus restricting $\ell =$e or μ for both leptons.

7.1 Event selection and reconstruction

The selection procedure starts from the $W^+W^- \to \overline{\ell}\nu_\ell\ell'\overline{\nu}_{\ell'}$ event sample used in the cross-section analysis. We then apply further cuts, mainly to suppress the contribution of events with one or two τ leptons which cannot be reconstructed. Only the 183 GeV sample is analysed, as the statistics in the lower energy samples are too small.

Simple cuts are applied to ensure that the momenta and charges of the two leptons can be determined. We require the events to have at least two reconstructed cones containing charged particle tracks passing the quality cuts used in the primary $\overline{\ell}\nu_\ell\ell'\overline{\nu}_{\ell'}$ selection. The two highest-energy cones with charged particle tracks are assigned to the leptons and the charge of each cone is found by summing the charges of the tracks in the cone. The charges of the cones are required to be of different signs, or if one cone has a zero charge, the other must have a non-zero charge.

At this stage, 52% of the selected sample consists of events with at least one $W \to \tau\nu$ decay. This fraction is suppressed by the following selections:

- The highest track momentum, p_1, in each lepton cone must exceed 23.0 GeV, which is less by approximately twice the experimental resolution than the minimum momentum allowed for a lepton from an on-shell W decay in an event with no ISR at $\sqrt{s}$=183 GeV.
- The two lepton cones must each have no more than two good electromagnetic clusters [47].
- Each of the lepton cones must be classified as an electron or a muon candidate, using the momentum of the most energetic track in the cone (p_1), the electromagnetic calorimeter energy in the cone (E_{EM}), and the hadron calorimeter energy in the cone (E_{HC}), as follows:
  - electron candidate cones are required to have $E_{EM}/p_1 > 0.75$ and $E_{HC}/p_1 < 0.1$,
  - muon candidate cones are required to have $E_{EM}/p_1 < 0.1$ and $E_{HC}/p_1 < 0.5$.

After applying these τ rejection cuts, the contamination from events with $W \to \tau\nu$ decays falls to 10%. This fraction is found to be essentially independent of the TGC parameters.

In the data, 78 events are selected by the primary $\bar{\ell}\nu_\ell \ell' \bar{\nu}_{\ell'}$ selection. Of these, 74 events pass the simple charge/momentum reconstruction requirements, and 30 pass also the τ rejection selections. The purity of events with two charged leptons (e, μ or τ) and two neutrinos in this final sample is predicted to be above 99%, where the main background (0.13±0.07 events) comes from the reaction $e^+e^- \to e^+e^-\mu^+\mu^-$. This level of background is negligible and is not considered further.

The lepton momenta are reconstructed using the track momentum for muon candidate cones, and the energy seen in the electromagnetic calorimeter for electron candidate cones.

The five characteristic angles are reconstructed event by event, in the approximation of zero W width and no ISR. This means that the two $\ell\nu$ systems are taken to have the W mass and the two W systems are assumed to recoil back-to-back in the laboratory frame, with a total energy equal to the centre-of-mass energy. When these constraints are applied, the six observed momentum components of the two charged leptons can be transformed into the five angles (plus an overall azimuthal angle which is of no interest). However, this transformation requires the solution of a quadratic equation, and thus there are either two, or no, real solutions for any specific event. The angle set $\{\cos\theta_W$, ϕ_1^* and $\phi_2^*\}$ suffers from this ambiguity, but θ_1^* and θ_2^* can be determined from the magnitudes of the lepton momenta alone. In the ideal case, where the W bosons are produced on-shell, and where there are no ISR or detector resolution effects, all events have two solutions: the ambiguity corresponds to a reflection ambiguity for the two neutrinos in the plane defined by the two charged lepton momentum vectors. The effects of W width, ISR and detector smearing can move leptons to momentum configurations not allowed in on-shell W decays yielding complex solutions for the momenta when attempting to reconstruct the neutrinos. These events lie preferentially in certain regions of the five-angle space, and losing them from the analysis would introduce biases. They can be recovered simply by taking the nearest real solution in five-angle space, taken to be the complex neutrino momentum solution with the imaginary part set to zero. In these cases there is exactly one nearest real solution: the two solutions with complex momenta are complex conjugates of each other.

Of the 30 selected candidates, 21 have two solutions found and the other 9 have their angular information recovered using the nearest real solution prescription. This is consistent with the Monte Carlo expectation of 8.9 events failing to have two reconstructed solutions.

7.2 TGC analysis

The fit for a TGC parameter α consists of minimising $\log L$, defined as:

$$\log L = -\sum_{\text{events}} \log \left(\frac{\frac{d\sigma}{d\Omega}(\alpha)}{\int \frac{d\sigma}{d\Omega}(\alpha) f(\Omega) d\Omega} \right),$$

where Ω represents the five-angle set (equivalent to phase space for on-shell W bosons and no ISR) and f represents the acceptance, assumed to be independent of α (valid in the on-shell, no-ISR case). The differential cross-section $d\sigma/d\Omega$ is determined using the program of Bilenky *et al.* [3]. For events with two solutions for the five angles, the average of the differential cross-sections at the two solutions is used.

The advantage of this unbinned maximum likelihood approach over binned techniques, as employed in the $\mathrm{q\overline{q}q\overline{q}}$ and $\mathrm{q\overline{q}}\ell\nu_\ell$ channel analyses, is that it uses the full five-angle information without any loss of information from binning. The main disadvantage is that the naïve cross-section calculation of $d\sigma/d\Omega$ does not include many of the effects which really occur: specifically the effects of ISR and W width, detector resolution, and backgrounds. The detector and selection acceptance is partially included through the acceptance function $f(\Omega)$ via an approximate analytical acceptance model.

It is essential to demonstrate that this simple fit is effective in extracting couplings and that the effects not modelled in the fit function have a relatively small influence. The implications of unmodelled effects can be pernicious: they can give rise to biases in the fitted couplings and in the estimations of the fit errors. These issues are addressed via Monte Carlo tests, with high statistics to measure biases in the fit, and with large numbers of simulated low-statistics experiments to calibrate the errors.

Studies are made with high-statistics Monte Carlo samples to test the biases in the fit method. These biases can arise from a variety of causes and are examined step-by-step by considering Standard Model samples with different effects included. Biases and systematic errors are derived as described in the following, with results shown in Table 11. In all cases the systematic errors are chosen so as to cover the differences in Monte Carlo models and the full size of any bias observed. In most tests, events from different Monte Carlo generators gave consistent results and the exceptions are noted.

a) The effect of the primary $\overline{\ell}\nu_\ell\ell'\overline{\nu}_{\ell'}$ selection cuts is assessed by fitting with the true momenta of decay leptons, both before and after the selection cuts are applied, to fully simulated events. This test is made with Monte Carlo W-pair events generated by EXCALIBUR, grc4f and KoralW. The modelling of the main acceptance effects in the function f reduces the bias from the acceptance.

b) Fits are made using the same fully simulated events, but fitting both with the true and the reconstructed momenta.

c) The effect of the additional $W \to \tau\nu$ rejection cuts on the $\overline{\ell}\nu_\ell \ell' \overline{\nu}_{\ell'}$ signal (ℓ = e or μ) is assessed by fitting to the reconstructed simulated signal events before and after the cuts are applied.

d) The $W^- \to \tau\overline{\nu}_\tau$ background is next included, and the simulated samples refitted. The size of the bias, averaged over the Excalibur, grc4f and KoralW samples, was found to be small. In this case, however, the different generators do give differences which are on the edge of significance: Excalibur and grc4f indicate a small positive bias to the results, KoralW a slightly larger negative one. The systematic error shown in Table 11 was chosen to cover all the different predicted biases. The modelling of τ polarisation and decays is one area in which some of the generators are known to be defective, so that the different biases seen are not surprising: nonetheless we quote an error large enough to cover all three models.

e) Four-fermion effects were tested by fitting Excalibur and grc4f samples produced either including only the CC03 W-pair diagrams, or when all four-fermion diagrams contributing to $\overline{\ell}\nu_\ell \ell' \overline{\nu}_{\ell'}$ final states were employed, including the contributions from extra final states such as $\mu^+\mu^-\nu_e\bar{\nu}_e$. While the two Monte Carlo generators predict quite different changes in accepted cross-sections when the four-fermion effects are included, the shifts in fit results are small and compatible with each other. The central value of the bias was taken to be that of Excalibur, and is listed in Table 11. The larger of the magnitude of the bias, and the difference between the shifts seen with Excalibur and grc4f, is taken as the associated systematic error.

	Source	$\Delta\kappa_\gamma$	Δg_1^z	λ
a)	$\overline{\ell}\nu_\ell \ell' \overline{\nu}_{\ell'}$ selection	−0.03±0.12	+0.05±0.05	+0.01±0.05
b)	Detector resolution	−0.07±0.07	−0.05±0.05	−0.02±0.02
c)	τ rejection	−0.07±0.07	−0.05±0.05	−0.02±0.02
d)	τ background	+0.02±0.04	−0.01±0.07	−0.02±0.03
e)	4-fermion effects	−0.10±0.10	−0.01±0.02	−0.01±0.02
f)	Low statistics tests	±0.56	±0.05	±0.03
	Combined	−0.25±0.61	−0.07±0.14	−0.06±0.09
	log L correction factor	1.17	2.07	1.39

Table 11: Summary of biases, systematic errors and likelihood scale factors derived from Monte Carlo tests for fits to the $\overline{\ell}\nu_\ell \ell' \overline{\nu}_{\ell'}$ angular distribution. Rows a) to f) show biases derived from the different tests discussed in the text, together with the associated systematic errors. The last row shows the log-likelihood scale correction applied.

In addition to these detailed studies with Standard Model events, high-statistics bias tests were also made for non-standard couplings, to ensure that the fit biases are not changing strongly with the underlying TGCs. These tests were done separately for W-pair and full four-fermion samples. In most cases, the best fits were obtained with values consistent with the generated couplings. Some fits, particularly for $\Delta\kappa_\gamma$, show an additional minimum separated from the correct value, and in some cases this may fit slightly better than the generated coupling value. In one case ($\Delta\kappa_\gamma$=1 with the full four-fermion diagrams) the two minima merge. In all cases the true generated coupling was excluded by an amount equivalent to a $\log L$ interval of less than 0.25, with the present statistics. Incorrect second minima would in any case be removed in the full analysis by the addition of the event rate information and that from the other channels.

The high-statistics studies described above evaluate the biases intrinsic to the unbinned maximum likelihood fit method. It is also essential for this fitting approach to calibrate the fit errors, as they cannot be expected to be estimated free of bias. This is done in the same way as for the other decay channels, using many Monte Carlo subsamples with the same statistics as the data (30 event). A scale correction to the $\log L$ function is calculated such that in 68% of the subsamples the correct TGC value is inside the error interval. The scale corrections are listed in Table 11.

The mean of the central values of these low-statistics fits were also compared, for each model, with the expected bias from the high-statistics test. The results are consistent for Δg_1^z and λ but differ by 0.56 for $\Delta\kappa_\gamma$. The larger of the differences or the statistical precision of the test is quoted as the "low statistics tests" systematic error, f), in Table 11.

7.3 Results for the $\overline{\ell}\nu_\ell\ell'\overline{\nu}_{\ell'}$ channel

The reconstructed $\cos\theta_{\mathrm{W}}$ distribution is shown in Figure 9 and compared with the Standard Model expectation and different TGC hypotheses. The statistics is low, but the shape is consistent with the Standard Model expectation, as is the joint distribution of $\cos\theta_1^*$ and $\cos\theta_2^*$ shown in Figure 10. In both figures there is a clear difference visible between the different high-statistics Monte Carlo predictions. It is interesting to note that the correlation between the two θ_i^* angles changes with λ. Such an effect can only be measured well in the $\overline{\ell}\nu_\ell\ell'\overline{\nu}_{\ell'}$ channel because of the difficulty in distinguishing the quark from the antiquark direction when a W boson decays hadronically.

Level of results	$\Delta\kappa_\gamma$	Δg_1^z	λ
Without systematics	$-1.00^{+0.94}_{-0.92}$	$-0.79^{+0.56}_{-0.69}$	$-0.29^{+0.34}_{-0.38}$
Expected errors	±1.08	±0.71	±0.41
Including systematics	$-0.74^{+1.23}_{-1.16}$	$-0.76^{+0.70}_{-0.79}$	$-0.23^{+0.35}_{-0.39}$
Including cross-section	$-0.30^{+1.00}_{-0.72}$	$-0.29^{+0.44}_{-0.31}$	$-0.18^{+0.32}_{-0.30}$

Table 12: Fit results at different levels, in the $\overline{\ell}\nu_\ell\ell'\overline{\nu}_{\ell'}$ channel.

The results of the fits to the 30 selected candidates are listed in the first row of Table 12. These results do not include any systematic errors but they correspond to the $\log L$ curves after adjustment with the scale factor to obtain the correct statistical errors. The expected errors, defined to be the r.m.s. values of the Monte Carlo subsample results, are listed in the second row of Table 12 and they are comparable with the statistical errors obtained from the corrected $\log L$ functions.

In the next step, the $\log L$ functions are shifted to correct for the biases and convolved with the combined systematic uncertainties. The results are listed in the third row of Table 12. Finally, the results are combined with those of the cross-section analysis corresponding to the $\overline{\ell}\nu_\ell \ell' \overline{\nu}_{\ell'}$ channel and using the 161, 172 and 183 GeV data samples. This combination is done by adding the corresponding log-likelihood curves, and the results are listed in the last row of Table 12.

8 Combined TGC results

The TGC results for the three event selections using the angular distributions are combined by summing the corresponding $\log L$ functions. The correlation between the systematic errors of the three results is neglected, since most of the important sources of systematic errors are relevant to a particular result and not common to all three of them. The $\log L$ functions obtained for the different couplings are shown in Figure 12. Adding these functions to those obtained using the total cross-section yields the combined $\log L$ functions which are plotted in Figure 12. Table 13 lists the combined results.

	$\Delta\kappa_\gamma$	Δg_1^z	λ
Combined results	$0.11^{+0.52}_{-0.37}$	$0.01^{+0.13}_{-0.12}$	$-0.10^{+0.13}_{-0.12}$
95% C.L. limits	[–0.55, 1.28]	[–0.23, 0.26]	[–0.33, 0.16]

Table 13: Combined results of the three TGC parameters. The result on each parameter is obtained setting the other two parameters to zero.

To study correlations between the three TGC parameters we also extract the $\log L$ as a function of all three variables, $\Delta\kappa_\gamma$, Δg_1^z and λ. Figure 13 shows the 95% C.L. contour plots obtained from two-dimensional fits, where the third parameter is fixed at its Standard Model value of zero. We also perform a three-dimensional fit, where all three couplings are allowed to vary simultaneously. The corresponding projections are plotted as dashed contour lines in Figure 13. As can be seen, the allowed range for each parameter is extended when the constraints on the other two parameters are removed.

These three-dimensional fits can be used to obtain results for any other set of TGC parameters, as long as relations (1) between the five couplings are satisfied. For example, we determine the α parameters used in our previous publications [9, 11] to be $\alpha_{B\phi}=0.11^{+0.52}_{-0.37}$, $\alpha_{W\phi}=-0.04 \pm 0.09$ and $\alpha_W=-0.10^{+0.13}_{-0.12}$. The result on each α parameter is obtained assuming that the other two parameters vanish.

9 Summary and conclusions

Using a sample of 877 W^+W^- candidates collected at LEP at a centre-of-mass energy of 183 GeV, we measure the total cross-section of,

$$\sigma(e^+e^-\to W^+W^-) = 15.43 \pm 0.61 \pm 0.26 \text{ pb}$$

under the assumption that the W boson decay branching fractions and distributions of production and decay angles are all according to the Standard Model expectations.

A measurement of the W branching fractions is made using the combined 161 GeV, 172 GeV and 183 GeV data samples. The results for the different leptonic decay channels are consistent with each other, as expected from lepton universality. Assuming Standard Model total cross-section and lepton universality, we obtain the hadronic decay fraction to be $(67.9 \pm 1.2 \pm 0.5)\%$. From this result, a value for the CKM mixing matrix elements $|V_{cs}| = 0.99 \pm 0.06 \pm 0.02$ is extracted, using also the measurements of the other matrix elements not involving the top quark.

The total cross-section measurement, being consistent with the Standard Model prediction of 15.72 pb^{-1}, can be used to place limits on anomalous triple gauge boson couplings. Those couplings are also investigated in an independent way, using the W-pair production and decay angular distributions for $q\overline{q}\overline{\ell}\nu_\ell$, $q\overline{q}q\overline{q}$ and $\overline{\ell}\nu_\ell\ell'\overline{\nu}_{\ell'}$ final states. The $W^+W^-\to q\overline{q}\overline{\ell}\nu_\ell$, being the most sensitive channel for this study, is analysed by three different methods, one of them utilising for the first time the spin density matrix of the W decay. All three methods lead to consistent results. The spin density matrix is used to measure the cross-sections to produce transversely and longitudinally polarised W bosons. Integrating over all angles, the fraction of longitudinally polarised W bosons is determined to be $0.242 \pm 0.091 \pm 0.023$.

The TGC measurements for all decay channels are combined, and the results obtained are,

$$\begin{aligned}
\Delta\kappa_\gamma &= +0.11^{+0.52}_{-0.37}, \\
\Delta g_1^z &= +0.01^{+0.13}_{-0.12}, \\
\lambda &= -0.10^{+0.13}_{-0.12},
\end{aligned}$$

where each parameter is determined setting the other two parameters to zero. The precision of these results is comparable to the latest D0 results obtained from boson pair production at the Tevatron $\overline{p}p$ collider [8]. These results supersede those from our previous publications [9, 11]. They are all consistent with the Standard Model value of zero.

Acknowledgements

We thank T. Wiseman for his contribution to this analysis.
We particularly wish to thank the SL Division for the efficient operation of the LEP accelerator at all energies and for their continuing close cooperation with our experimental group. We thank our colleagues from CEA, DAPNIA/SPP, CE-Saclay for their efforts over the years on the time-of-flight and trigger systems which we continue to use. In addition to the support staff

at our own institutions we are pleased to acknowledge the
Department of Energy, USA,
National Science Foundation, USA,
Particle Physics and Astronomy Research Council, UK,
Natural Sciences and Engineering Research Council, Canada,
Israel Science Foundation, administered by the Israel Academy of Science and Humanities,
Minerva Gesellschaft,
Benoziyo Center for High Energy Physics,
Japanese Ministry of Education, Science and Culture (the Monbusho) and a grant under the Monbusho International Science Research Program,
Japanese Society for the Promotion of Science (JSPS),
German Israeli Bi-national Science Foundation (GIF),
Bundesministerium für Bildung, Wissenschaft, Forschung und Technologie, Germany,
National Research Council of Canada,
Research Corporation, USA,
Hungarian Foundation for Scientific Research, OTKA T-016660, T023793 and OTKA F-023259.

References

[1] Physics at LEP2, edited by G. Altarelli, T. Sjöstrand and F. Zwirner, CERN 96-01 Vol. 1, 525.

[2] K. Hagiwara, R.D. Peccei, D. Zeppenfeld and K. Hikasa, Nucl. Phys. **B282** (1987) 253.

[3] M. Bilenky, J.L. Kneur, F.M. Renard and D. Schildknecht, Nucl. Phys. **B409** (1993) 22; Nucl. Phys. **B419** (1994) 240.

[4] K. Gaemers and G. Gounaris, Z. Phys. **C1** (1979) 259.

[5] A. De Rujula, M.B. Gavela, P. Hernandez and E. Masso, Nucl. Phys. **B384** (1992) 3.

[6] K. Hagiwara, S. Ishihara, R. Szalapski and D. Zeppenfeld, Phys. Lett. **B283** (1992) 353; Phys. Rev. **D48** (1993) 2182.

[7] CDF Collaboration, F. Abe *et al.*, Phys. Rev. Lett. **78** (1997) 4536.

[8] D0 Collaboration, B. Abbott *et al.*, Phys. Rev. **D58** (1998) 31102.

[9] OPAL Collaboration, K. Ackerstaff *et al.*, Phys. Lett. **B397** (1997) 147.

[10] DELPHI Collaboration, P. Abreu *et al.*, Phys. Lett. **B397** (1997) 158;
L3 Collaboration, M. Acciarri *et al.*, Phys. Lett. **B398** (1997) 223.

[11] OPAL Collaboration, K. Ackerstaff *et al.*, Eur. Phys. J. **C2** (1998) 597.

[12] L3 Collaboration, M. Acciarri *et al.*, Phys. Lett. **B413** (1997) 176;
DELPHI Collaboration, P. Abreu *et al.*, Phys. Lett. **B423** (1998) 194;
ALEPH Collaboration, R. Barate *et al.*, Phys. Lett. **B422** (1998) 369.

[13] R.L. Sekulin, Phys. Lett. **B338** (1994) 369.

[14] OPAL Collaboration, K. Ahmet *et al.*, Nucl. Instr. Meth. **A305** (1991) 275;
S. Anderson *et al.*, Nucl. Instr. Meth. **A403** (1998) 326.

[15] B.E. Anderson *et al.*, IEEE Transactions on Nuclear Science, **41** (1994) 845.

[16] D. Bardin *et al.*, Nucl. Phys. B, Proc. Suppl. **37B** (1994) 148;
D. Bardin *et al.*, "GENTLE/4fan v. 2.0: A Program for the Semi-Analytic Calculation of Predictions for the Process $e^+e^-\to 4f$", DESY 96-233, hep-ph/9612409.

[17] D0 Collaboration, B. Abbott *et al.*, Phys. Rev. Lett. **80** (1998) 3008;
CDF Collaboration, F. Abe *et al.*, Phys. Rev. Lett. **75** (1995) 11.

[18] J. Allison *et al.*, Nucl. Instr. Meth. **A317** (1992) 47.

[19] M. Skrzypek *et al.*, Comp. Phys. Comm. **94** (1996) 216;
M. Skrzypek *et al.*, Phys. Lett. **B372** (1996) 289.

[20] F.A. Berends, R.Pittau and R. Kleiss, Comp. Phys. Comm. **85** (1995) 437;
F.A. Berends and A.I. van Sighem, Nucl. Phys. **B454** (1995) 467.

[21] J. Fujimoto *et al.*, Comp. Phys. Comm. **100** (1997) 128.

[22] T. Sjöstrand, Comp. Phys. Comm. **82** (1994) 74.

[23] G. Marchesini *et al.*, Comp. Phys. Comm. **67** (1992) 465.

[24] S. Jadach *et al.*, Comp. Phys. Comm. **79** (1994) 503.

[25] S. Jadach, W. Placzek and B.F.L. Ward, Phys. Lett. **B390** (1997) 298.

[26] R. Engel, Z. Phys. **C66** (1995) 203;
R. Engel and J. Ranft, Phys. Rev. **D54** (1996) 4244.

[27] J.A.M. Vermaseren, Nucl. Phys. **B229** (1983) 347.

[28] OPAL Collaboration, K. Ackerstaff *et al.*, Eur. Phys. J. **C1** (1998) 395.

[29] OPAL Collaboration, K. Ackerstaff *et al.*, Eur. Phys. J. **C4** (1998) 47.

[30] OPAL Collaboration, K. Ackerstaff *et al.*, CERN-EP/98-108, to be published in Eur. Phys. J. C.

[31] OPAL Collaboration, G. Alexander *et al.*, Z. Phys. **C52** (1991) 175.

[32] N. Brown and W.J. Stirling, Phys. Lett. **B252** (1990) 657;
S. Catani *et al.*, Phys. Lett. **B269** (1991) 432;
S. Bethke, Z. Kunszt, D. Soper and W.J. Stirling, Nucl. Phys. **B370** (1992) 310;
N. Brown and W.J. Stirling, Z. Phys. **C53** (1992) 629.

[33] OPAL Collaboration, M.Z. Akrawy *et al.*, Phys. Lett. **B253** (1990) 511.

[34] S. Catani and M.H. Seymour, Phys. Lett. **B378** (1996) 287.

[35] R.K. Ellis, D.A. Ross and A.E. Terrano, Nucl. Phys. **B178** (1981) 421.

[36] O. Nachtmann and A. Reiter, Z. Phys. **C16** (1982) 45;
M. Bengtsson, Z. Phys. **C42** (1989) 75.

[37] D. Karlen, physics/9805018, Computers in Physics **12** (1998) 380.

[38] OPAL Collaboration, G. Alexander *et al.*, Z. Phys. **C69** (1996) 543.

[39] C. Caso *et al.*, Eur. Phys. J. **C3** (1998) 1.

[40] OPAL Collaboration, K. Ackerstaff *et al.*, Phys. Lett. **B389** (1996) 416.

[41] M. Davier, L. Duflot, F. LeDiberder and A. Rouge, Phys. Lett. **B306** (1993) 411;
M. Diehl and O. Nachtmann, Z. Phys. **C62** (1994) 397.

[42] R. Barlow and C. Beeston, Comp. Phys. Comm. **77** (1993) 219.

[43] G. Gounaris, J. Layssac, G. Moultaka and F.M. Renard, Int. J. Mod. Phys. **A19** (1993) 3285.

[44] L. Lönnblad and T. Sjöstrand, Eur. Phys. J. **C2** (1998) 165.

[45] T. Sjöstrand and V.A. Khoze, Z. Phys. **C62** (1993) 281.

[46] L. Lönnblad, Comp. Phys. Comm. **71** (1992) 15.

[47] OPAL Collaboration, G. Alexander *et al.*, Z. Phys. **C72** (1996) 191.

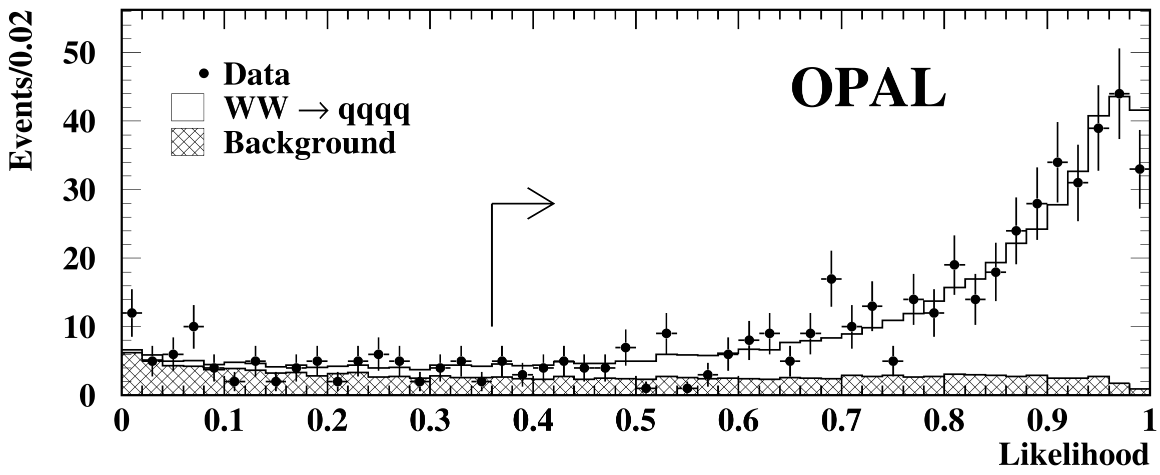

Figure 1: *The distribution of the likelihood discriminant used to select events in the* $W^+W^- \to q\overline{q}q\overline{q}$ *selection is shown for all preselected events. The points indicate the data and the histogram represents the Monte Carlo expectation where the hatched area shows the estimated contribution of the total background. The selection cut is indicated by the arrow.*

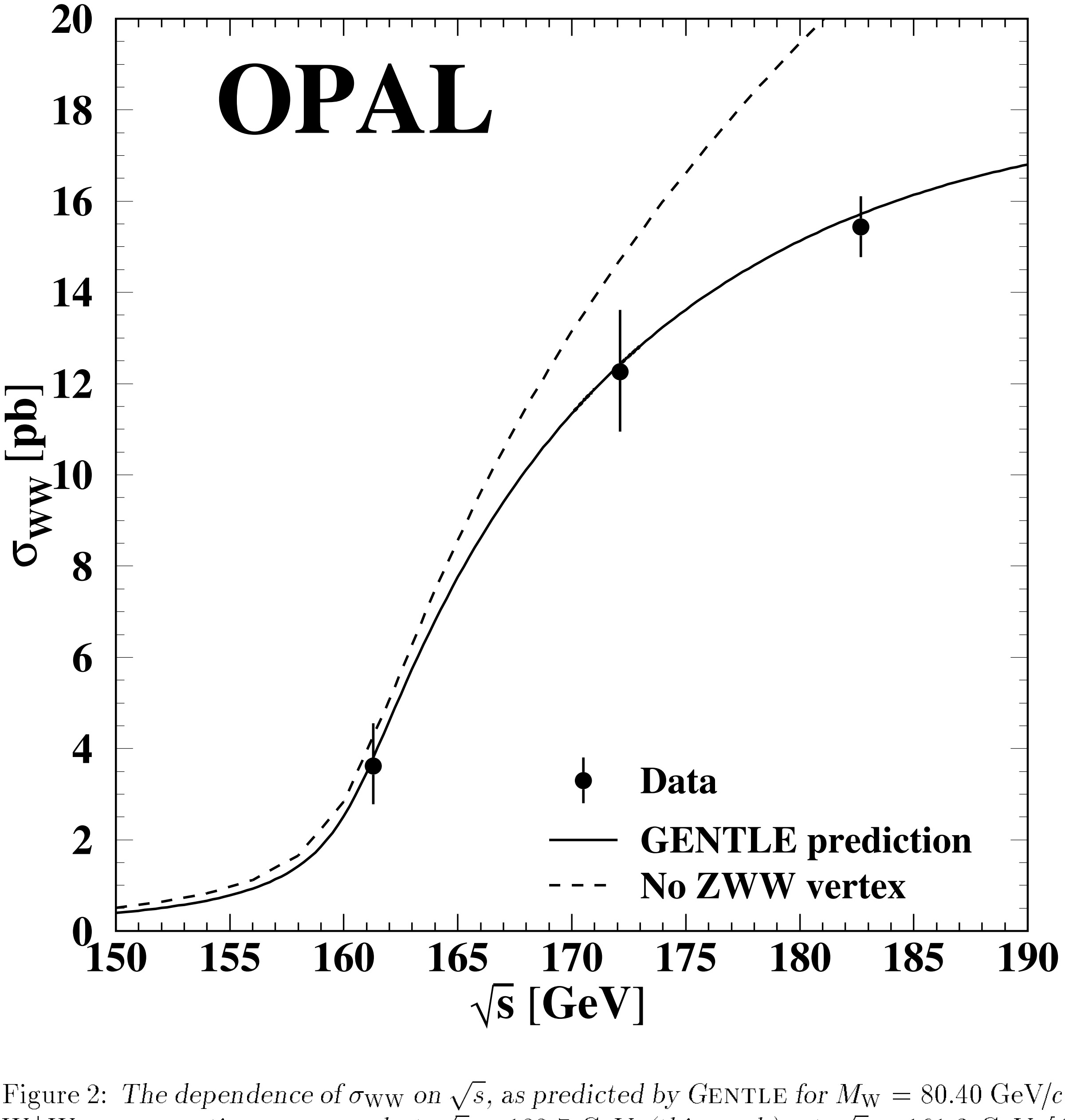

Figure 2: *The dependence of σ_{WW} on $\sqrt{s}$, as predicted by* Gentle *for $M_{\mathrm{W}} = 80.40$ GeV/c^2. The* $\mathrm{W^+W^-}$ *cross-sections measured at $\sqrt{s} = 182.7$ GeV (this work), at $\sqrt{s} = 161.3$ GeV [40] and $\sqrt{s} = 172.1$ GeV [28] are shown. The error bars include statistical and systematic contributions. The dashed curve shows the expected cross-section if the ZWW couplings are zero.*

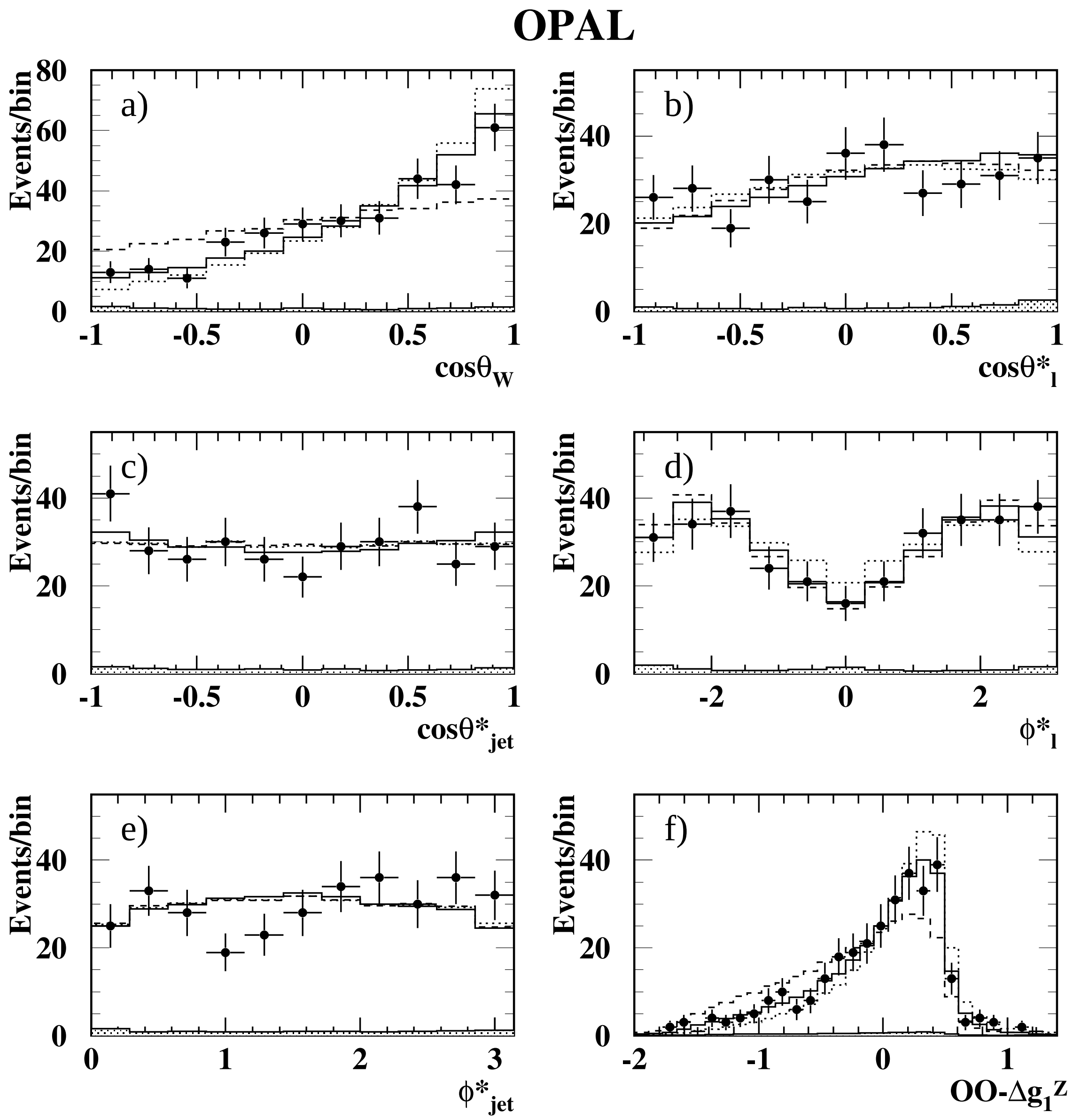

Figure 3: *Distributions of the kinematic variables* $\cos\theta_{\mathrm{W}}$, $\cos\theta^*_\ell$, $\cos\theta^*_{\mathrm{jet}}$, ϕ^*_ℓ, ϕ^*_{jet} *and the optimal observable corresponding to* Δg_1^{z}, *as obtained from the* $\mathrm{q\overline{q}}\ell\nu_\ell$ *events. The solid points represent the data. The histograms show the expectation of the Standard Model (solid line) and the cases of* Δg_1^{z}=+1 *and* −1 *(dotted and dashed lines respectively). The shaded histogram shows the non-*$\mathrm{q\overline{q}}\ell\nu_\ell$ *background. Notes: 1. In the case of* $W^+\to\bar{\ell}\nu$ *decays the value of* ϕ^*_ℓ *is shifted by* π *in order to overlay* W^+ *and* W^- *distributions in the same plot. 2. The jet with* $0 \le \phi^*_{\mathrm{jet}} \le \pi$ *is arbitrarily chosen as the quark (antiquark) jet from the decay of the* W^- (W^+).

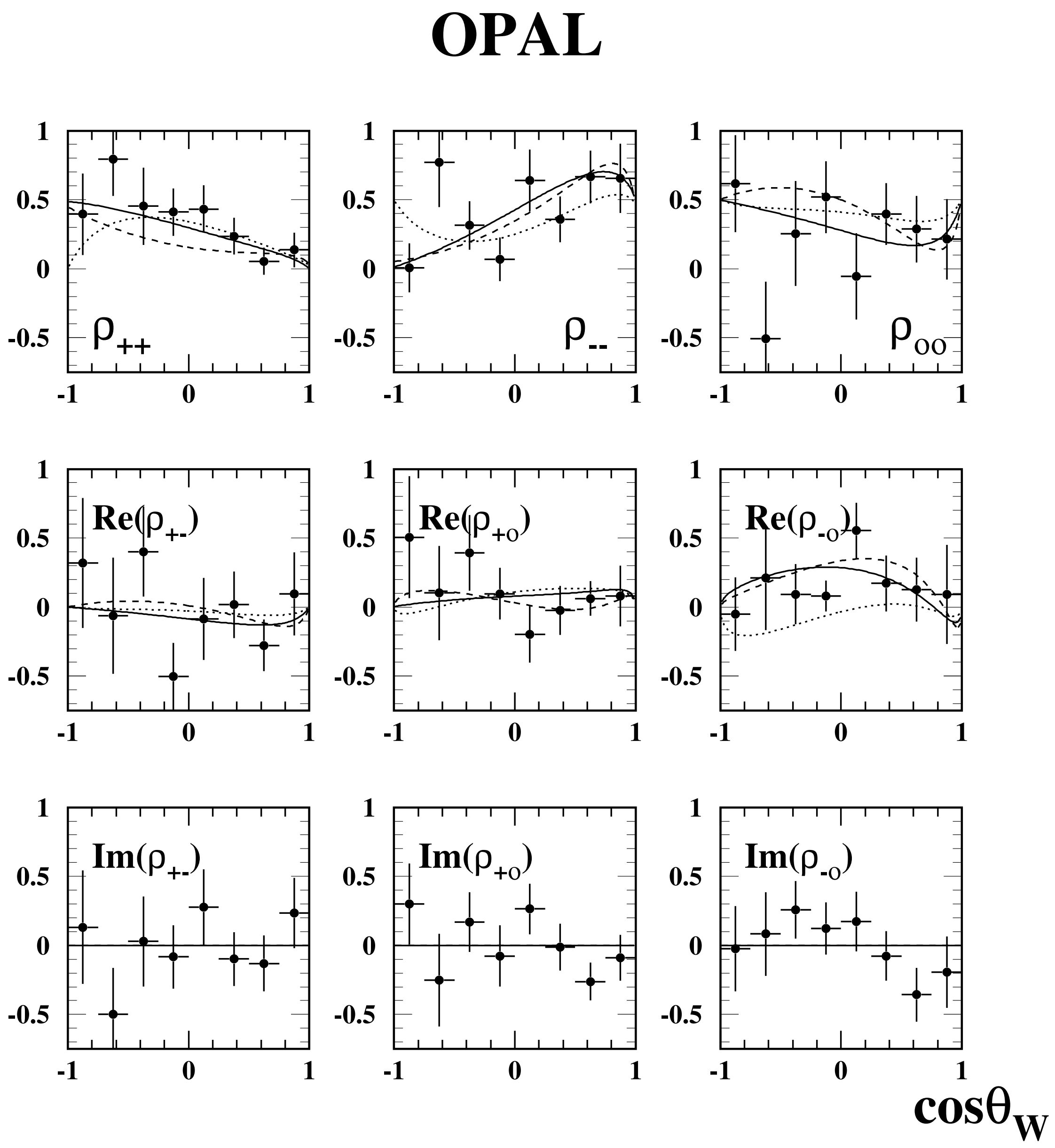

Figure 4: *Spin density matrix elements for the leptonically decaying W as a function of* $\cos\theta_{\mathrm{W}}$. *The data points are corrected for experimental effects. The solid (dotted, dashed) lines show the predictions of models with* Δg_1^z*=0 (+1, −1). All other anomalous couplings are set to zero.*

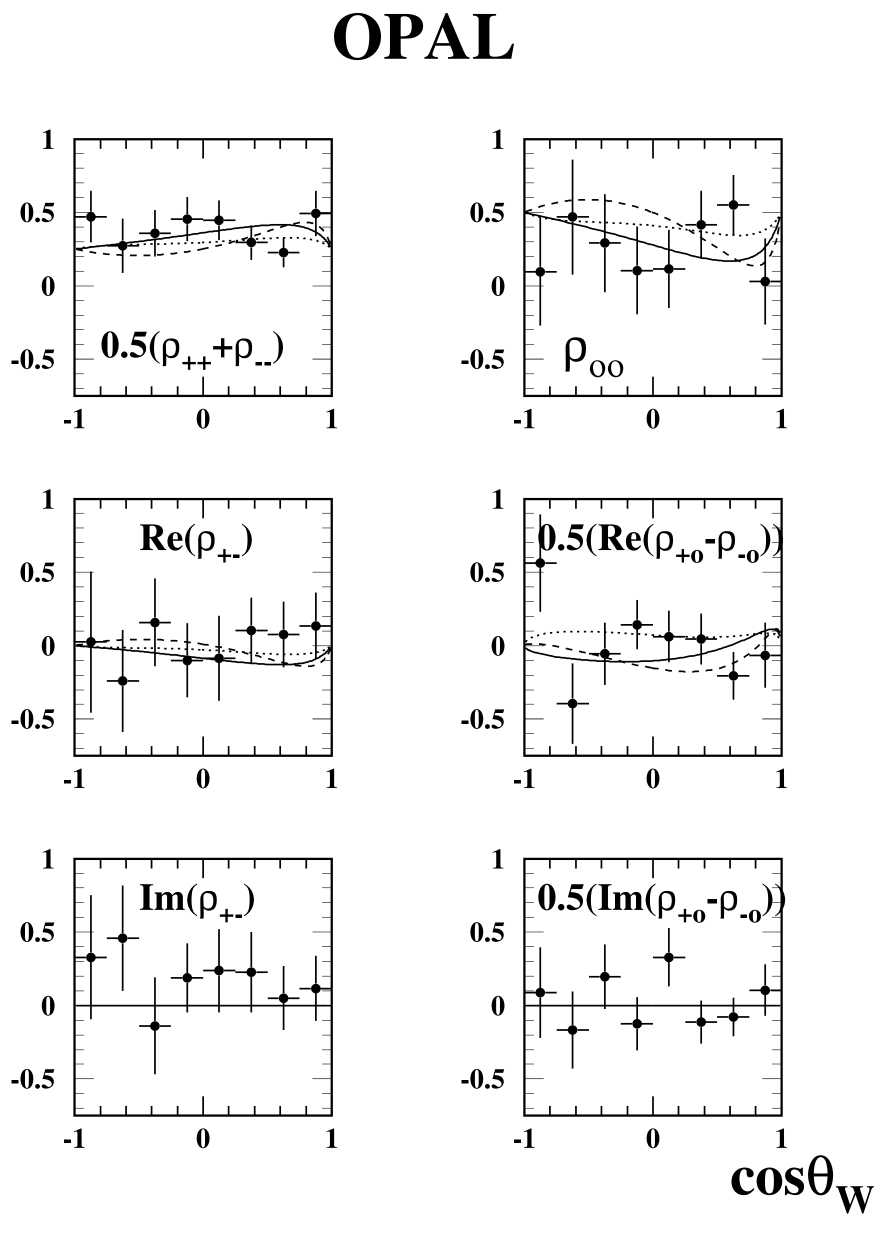

Figure 5: *Spin density matrix elements for the hadronically decaying W as a function of* $\cos\theta_{\mathrm{W}}$*. The data points are corrected for experimental effects. The solid (dotted, dashed) lines show the predictions of models with* Δg_1^z*=0 (+1, −1). All other anomalous couplings are set to zero.*

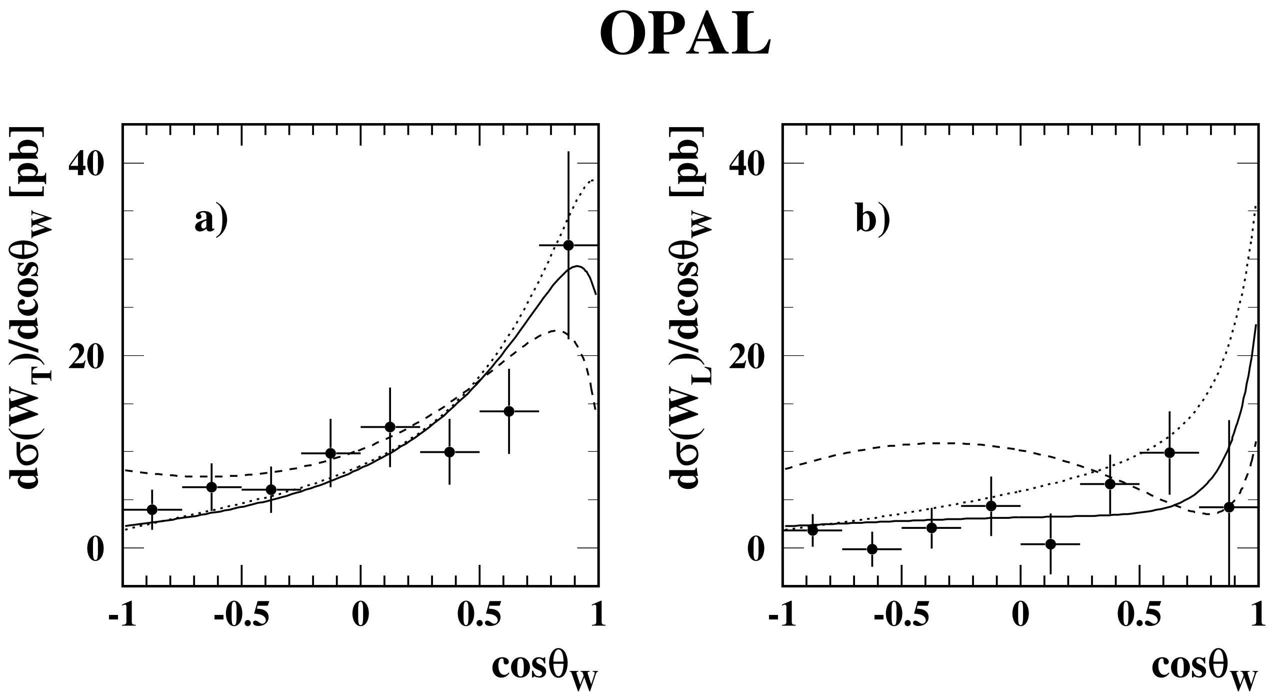

Figure 6: *Differential cross-section to produce a) a transversely polarised W and b) a longitudinally polarised W in a W-pair event where the second W can have any polarisation. The points represent the data and the solid (dotted, dashed) lines show the predictions of models with Δg_1^z=0 (+1, −1). The error bars include statistical and systematic uncertainties, except for a normalisation error of 4.3% associated with the total cross-section measurement.*

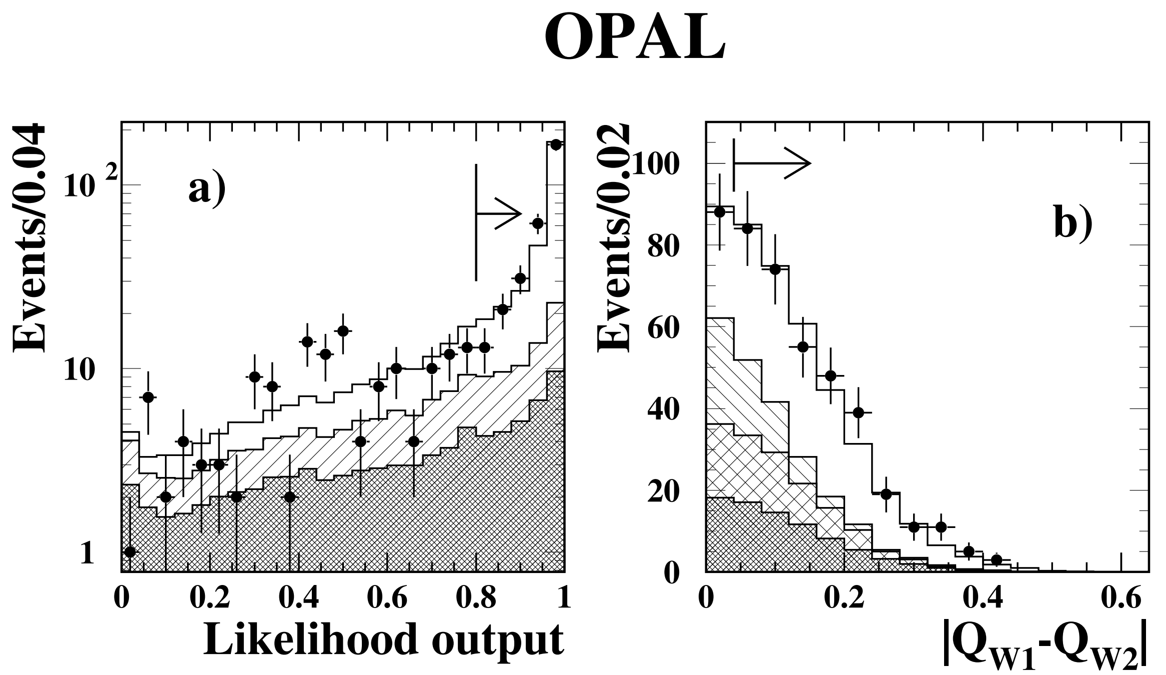

Figure 7: *For the* $q\bar{q}q\bar{q}$ *channel, a) distribution of the output of the jet-pairing likelihood corresponding to the most likely combination for the data collected at 183* GeV *(points) and for the Monte Carlo (histogram). The hatched area shows the contribution of wrong pairing, and the dark area represents the contribution of the background. The arrow indicates the cut value. b) Distribution of the charge separation of the W candidates for the data collected at 183* GeV *(points) and for the Monte Carlo (histogram). The hatched area shows the contribution of correct pairing and incorrect W charge, the double hatched area shows the contribution of wrong pairing, and the dark area represents the contribution of the background. The arrow indicates the cut value.*

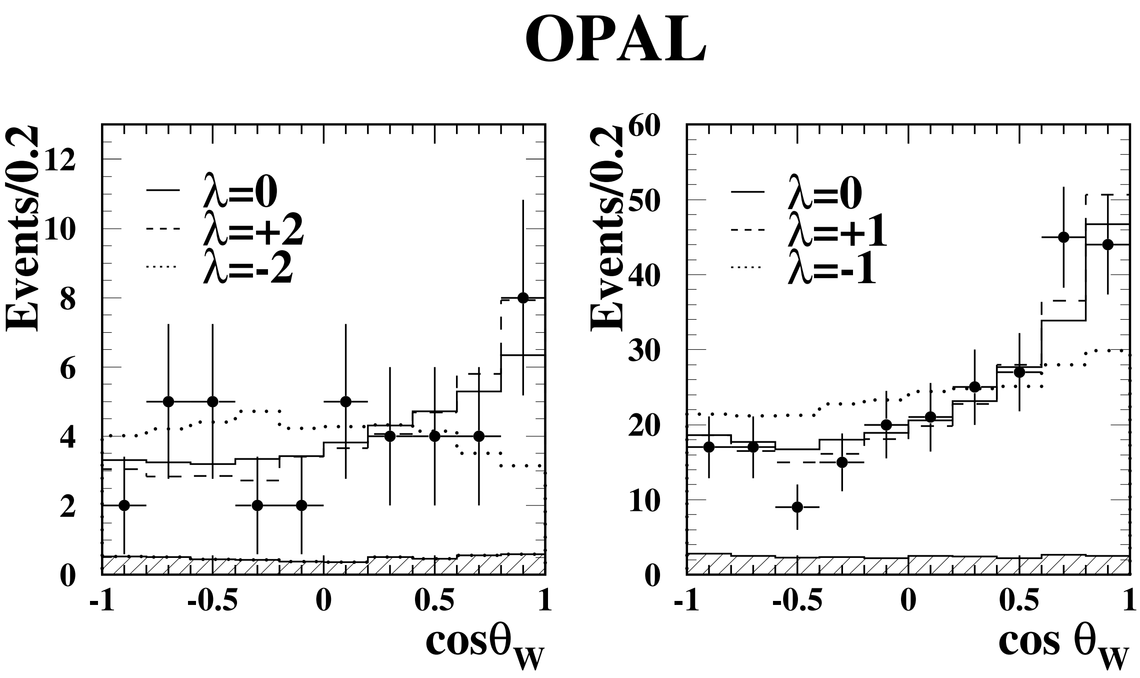

Figure 8: *Distribution of* $\cos\theta_{\mathrm{W}}$ *in* $\mathrm{q\overline{q}q\overline{q}}$ *events as obtained at 172* GeV *(left) and 183* GeV *(right). The solid points are the data. The Monte Carlo predictions for* λ*=0,+2,–2 and* λ*=0,+1,–1 are shown at 172 and 183* GeV*, respectively, as solid, dashed and dotted lines. The hatched histograms show the contributions of the* $\mathrm{Z}^0/\gamma \rightarrow \mathrm{q\overline{q}}$ *background, as predicted by* Pythia.

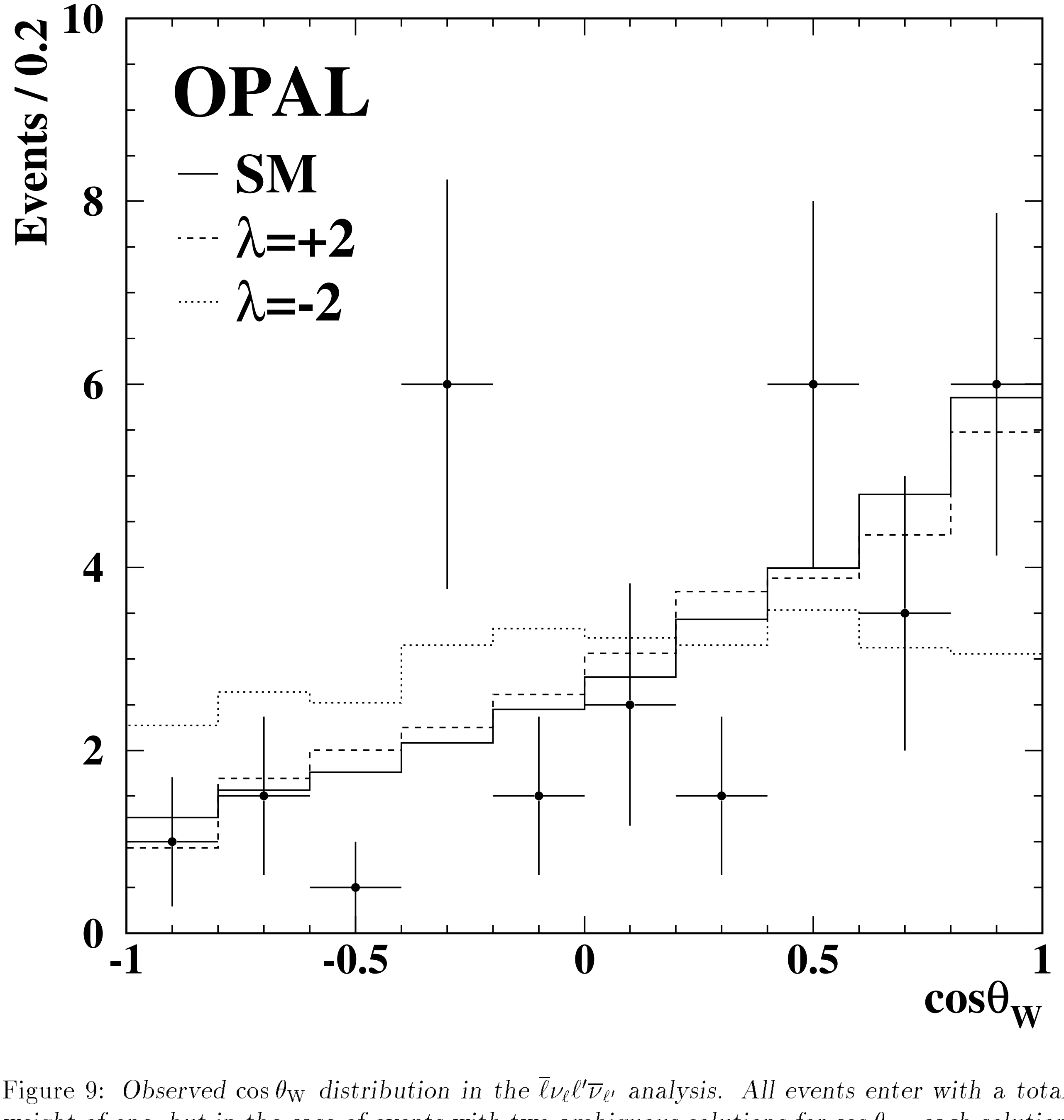

Figure 9: *Observed* $\cos\theta_{\mathrm{W}}$ *distribution in the* $\overline{\ell}\nu_\ell \ell'\overline{\nu}_{\ell'}$ *analysis. All events enter with a total weight of one, but in the case of events with two ambiguous solutions for* $\cos\theta_{\mathrm{W}}$*, each solution enters with a weight of 0.5.*

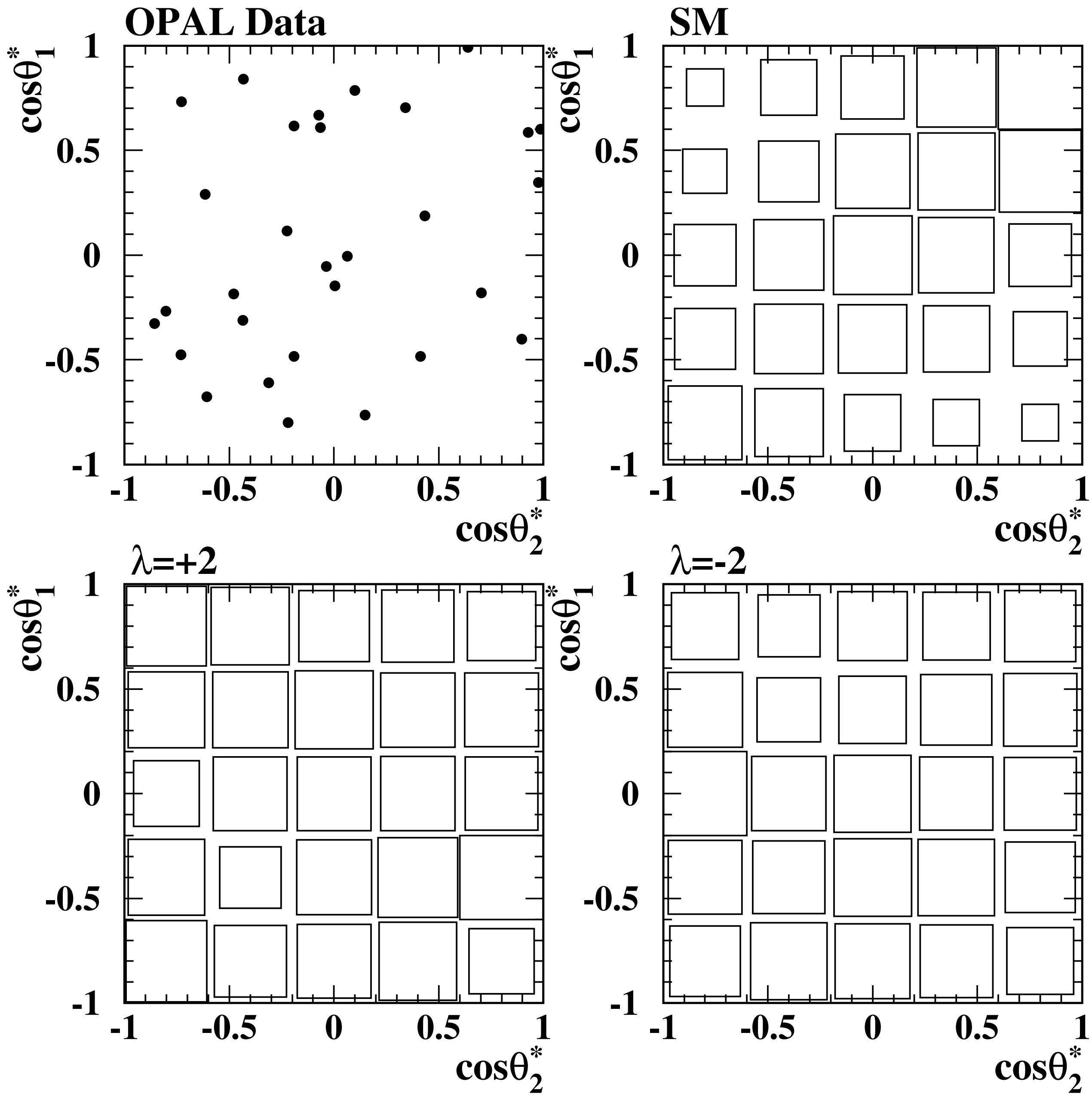

Figure 10: *Observed distribution of* $\cos\theta_1^*$ *vs.* $\cos\theta_2^*$ *in the* $\overline{\ell}\nu_\ell\ell'\overline{\nu}_{\ell'}$ *analysis, compared to the expected distributions from samples with standard (SM) and non-standard couplings, as indicated. In the panels corresponding to the Monte Carlo expectations, the area of each box is proportional to the fraction of the events falling into that bin.*

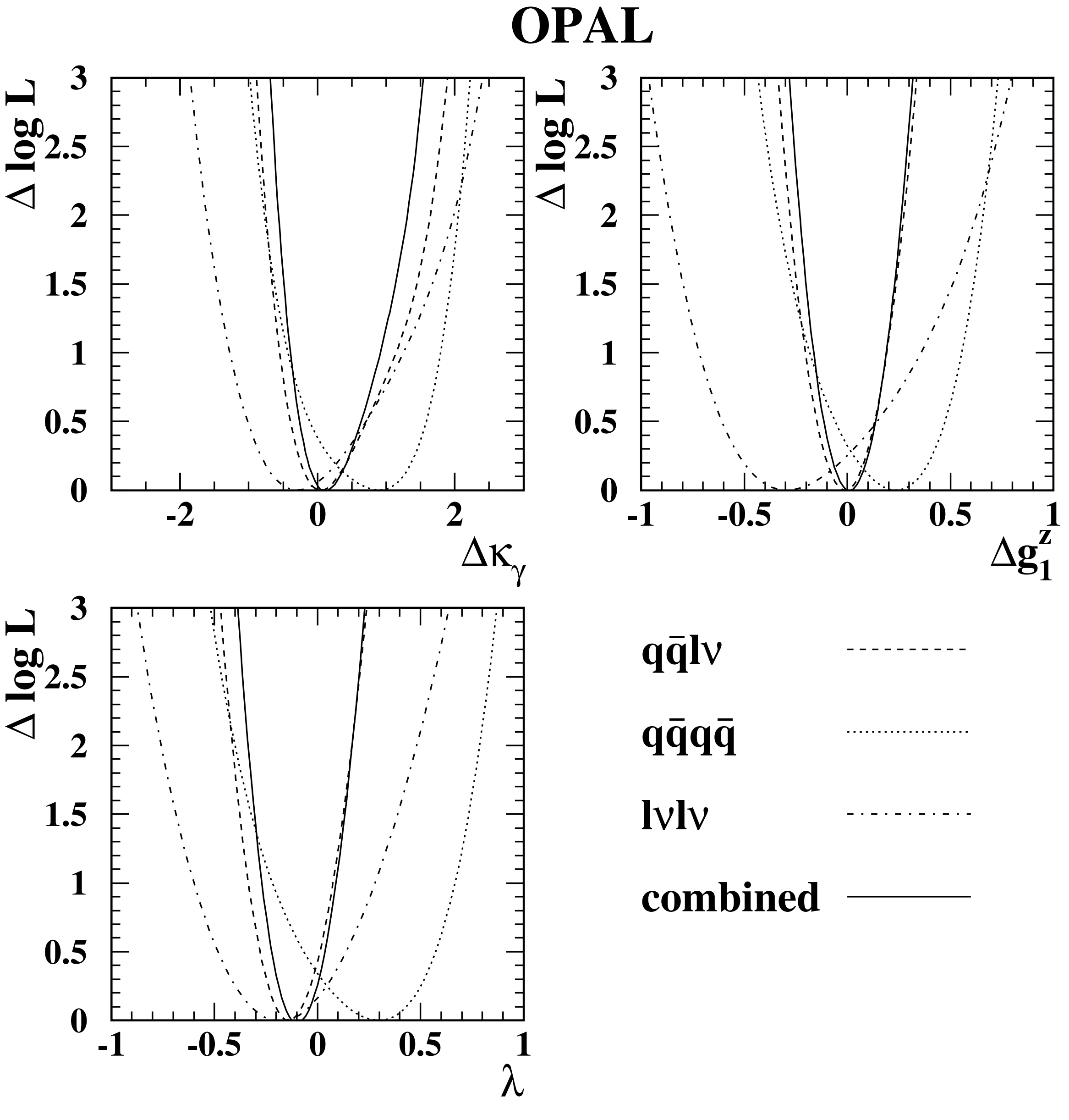

Figure 11: *Negative log-likelihood curves obtained in the different event selections:* $q\bar{q}\ell\nu_\ell$ *(dashed lines),* $q\bar{q}q\bar{q}$ *(dotted lines) and* $\bar{\ell}\nu_\ell\ell'\bar{\nu}_{\ell'}$ *(dash-dotted lines). Each curve is obtained by combining the results from the angular distributions and the cross-section and setting the other two* TGC *parameters to zero. Systematic errors are included. The solid line is obtained by combining the three event selections.*

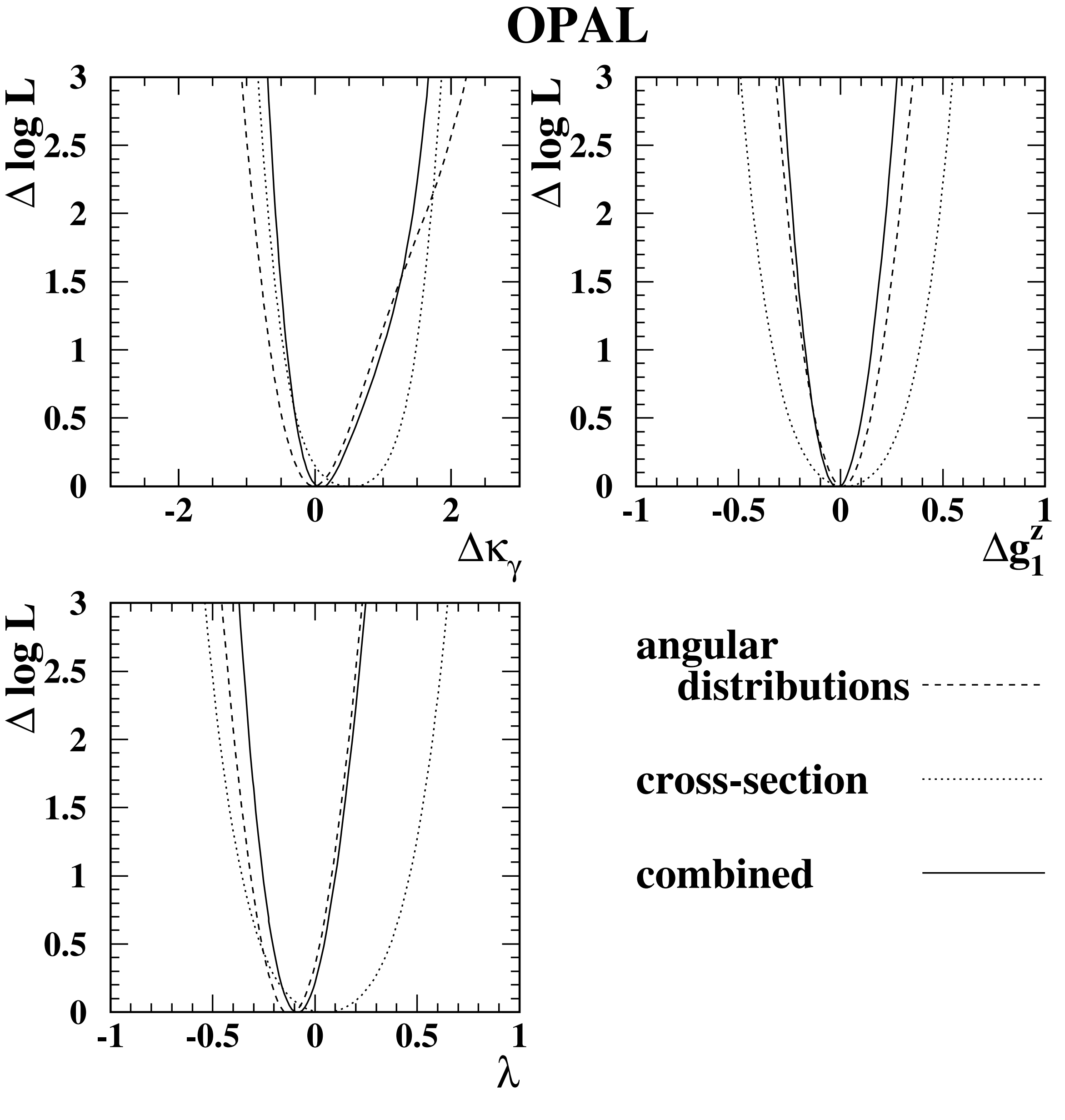

Figure 12: *Negative log-likelihood curves obtained using different sources of information on the TGCs. The curves for each TGC parameter are obtained setting the other two parameters to zero. The dashed lines are obtained from the angular distributions, and the dotted lines from the total cross-section. All W decay channels are used and systematic errors are included. The solid line is obtained by combining the two sources of information.*

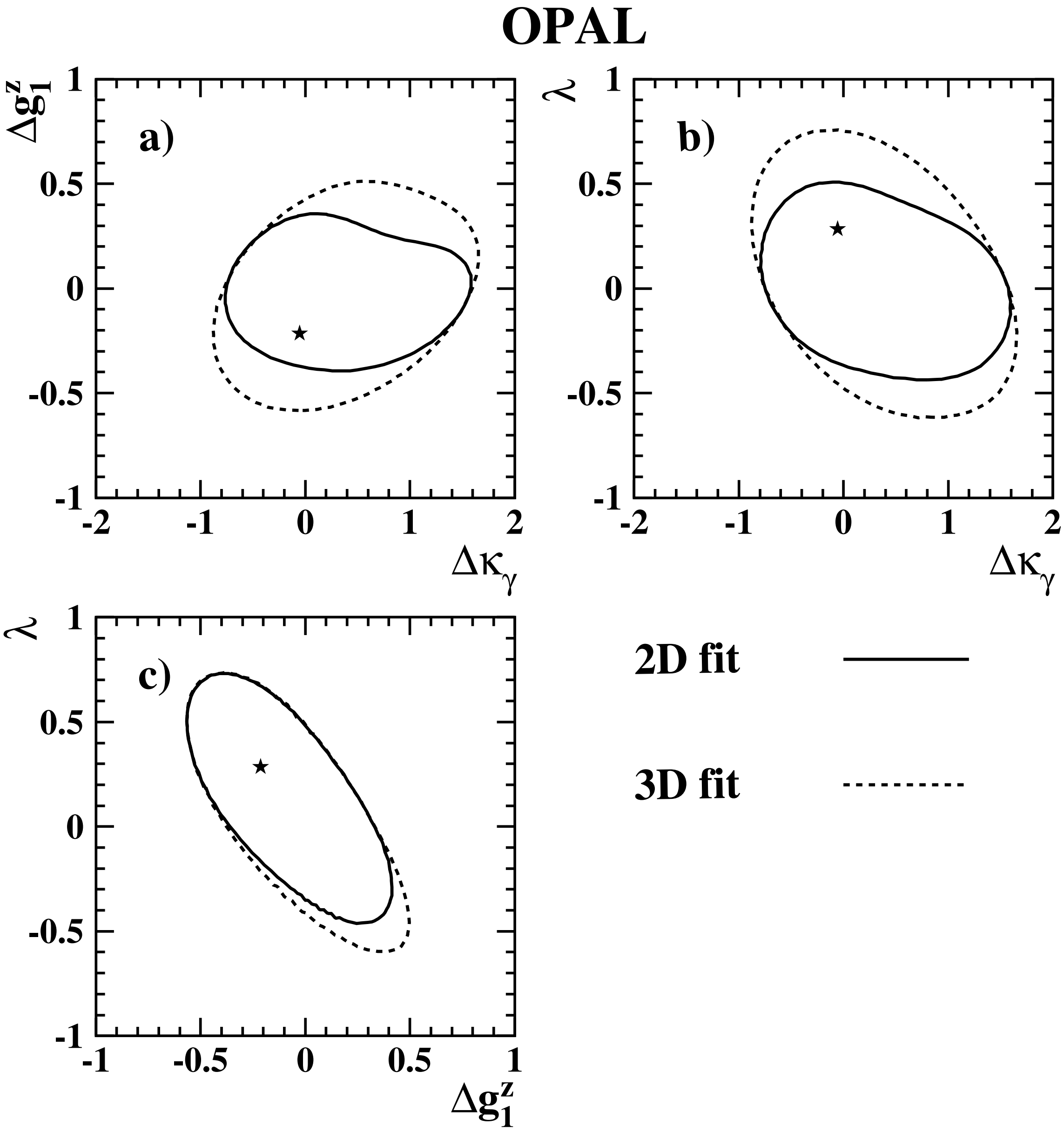

Figure 13: *The 95% C.L. two-dimensional correlation contours for different pairs of* TGC *parameters. The solid lines are obtained by varying two parameters and fixing the third one to zero, which is the Standard Model value. The dashed lines show the projections of the three-dimensional confidence regions obtained by varying all three parameters. The star indicates the best three-parameter fit values. These results are obtained from all cross-section data as well as angular distributions of all* $\mathrm{q\overline{q}}\ell\overline{\nu}_\ell$ *and 183 GeV* $\mathrm{q\overline{q}q\overline{q}}$ *data.*